



Assessment of spectral attributes in identifying gas hydrates in seismic data from the Pegasus Basin, offshore New Zealand

Emily Jackson¹ · Heather Bedle¹ · Thang Ha¹

Received: 12 May 2023 / Accepted: 30 September 2023 / Published online: 13 October 2023
© The Author(s), under exclusive licence to Springer Nature B.V. 2023

Abstract

Methane gas hydrates are formed in the subsurface along shallow ocean basins or in permafrost settings, and are commonly identified in the seismic data by the bottom-simulating reflector (BSR). Various methods have been employed in the past to measure gas hydrates from lab analyses, well log, or velocity data, but few studies have demonstrated methods to identify gas hydrates in seismic data when the BSR is sparse or lacking. One approach is to measure the expected attenuation caused by hydrates in the gas hydrate stability zone (GHSZ). Statistical attributes that measure the asymmetry of the seismic amplitude spectrum are applied to quantify the attenuation responses throughout the GHSZ. Although the study area does not contain well log data, there are numerous studies that confirm hydrates exist throughout the Pegasus Basin. These attributes, in addition to amplitude-related attributes, demonstrate that frequency-related variations are the major contributors to attenuation response, rather than seismic amplitude or geology effects. The spectral attribute results show that strong positive skewness and kurtosis variations above the high amplitude BSR is likely due to attenuation through an interval of hydrates. Negative skewness and kurtosis may correspond to an interval that does not contain hydrates, therefore suggesting that the GHSZ in the Pegasus Basin consists of discontinuous hydrates, rather than one continuous layer from ocean bottom to BSR.

Keywords Gas hydrates · Attenuation · Seismic data · Seismic attributes · Unsupervised machine learning

Introduction

Gas hydrates form in the shallow subsurface off-shore or in permafrost regimes at higher latitudes. They form under constrained high pressure and low temperature settings when water molecules trap gas molecules (usually methane) and freeze, forming a solid hydrate structure (Sloan 2003). Methane gas hydrates are emerging as a new energy horizon and have significant impact on engineering, climate and energy resources. Hydrates can pose significant risk during drilling oil and gas wells and while shear strength of the sediment increases with hydrate accumulation, dissociation of hydrates can lead to seafloor instability or slumping (Chand and Minshull 2004). Hydrates also have implications for climate concerns as widespread hydrate destabilization may result in the release significant volumes of gas into the ocean (Maslin et al. 2010). Estimates of gas bound within global

hydrate accumulations are 250,000 trillion cubic feet (Tcf), which is nearly 90% higher than total natural gas reserve estimates for the United States alone (US DOE, 2020; US EIA AEO, 2020), demonstrating the enormous magnitude of hydrates that exist globally. Nonetheless, the extent of hydrates and exact regimes of occurrence still contains significant uncertainty.

The pore-filling hydrates can form a seal, trapping migrating free gas in the zone below where hydrates fill the pore space of the rocks. The theoretical zone, modelled based on local pressure and temperature regimes, where hydrates are stable is called the gas hydrate stability zone, or GHSZ (Thomas et al. 1979). The base of the gas hydrate stability zone (BGHSZ) is sometimes signaled by an anomalous seismic reflector referred to as the bottom simulating reflector (BSR). In seismic reflection data, the BSR is observed as a negative impedance contrast between the hydrate-filled sediment zone and the free gas in the underlying zone (Singh et al. 1993; Dev and McMechan 2010; Davies et al. 2021). Hydrate-related BSRs have the opposite seismic polarity of the ocean bottom and track sub-parallel to the ocean bottom due to their approximate representation of a thermobaric

✉ Emily Jackson
emilyjackson@ou.edu

¹ University of Oklahoma School of Geoscience, Norman, OK, USA

boundary (Hornbach et al. 2003; Dvorkin et al. 2014). Hydrate BSRs are perhaps most evident when they cross-cut stratigraphy and feature high absolute seismic amplitudes (Hornbach et al. 2003). While the presence of a BSR is good indicator that hydrates exist in the subsurface, BSRs do not directly indicate the *concentration* of gas hydrate accumulations (Holbrook et al. 1996; Boswell et al. 2005). BSRs can also be due to processes unrelated to gas hydrate accumulation and trapped free gas (Sloan 2003), such as diagenesis of opal-A to opal-CT (Berndt et al. 2004). The absence of BSRs in a hydrate system can be due to lack of migrating gas in the system, failure of the hydrates to trap free gas, or depending on lithology, the impedance contrast between the hydrate filled sediments and non-hydrate filled sediments may not be large enough for a seismic reflector (Bedle 2019). Weak, discontinuous or absent BSRs complicate the process of identifying hydrates and require implementing other methods to image the extent of the gas hydrates (Chenin and Bedle 2020; Clairmont et al. 2021). Therefore, relying on clear BSRs alone in seismic data is unreliable (Holbrook et al. 1996; Majumdar et al. 2016), and other methods are often needed to confirm the existence of gas hydrates within the GHSZ.

A new method of detecting gas hydrates in seismic data is to use spectral shape seismic attributes to measure the attenuation in seismic frequencies that are caused by gas hydrates within the gas hydrate stability zone (Satyavani et al. 2008). Seismic frequencies naturally attenuate with depth; however, hydrates also attenuate the seismic frequencies. Although the exact mechanism has proven complex (Chand et al. 2004; Dvorkin et al. 2014), the attenuation of the seismic frequency should be visible in the seismic amplitude spectrum. Gas hydrates are shown to attenuate seismic waves from numerous seismic or well-based studies (e.g. Guerin and Goldberg, 2002; Chand and Minshull 2004; Dvorkin and Uden 2004; Sahoo et al. 2019), and this effect is even observed in synthetic seismic data created from real-world, hydrate-bearing well log data (Dvorkin et al. 2014). To quantify the attenuation response for both conventional and unconventional hydrocarbon accumulations, Li et al. (2015 and 2016) proposed skewness and kurtosis, two statistical measures, in combination with five other attenuation-related attributes, to measure attenuation in hydrocarbon-saturated reservoirs. Their research showed that the high attenuation generally correlated with high productivity in the gas-producing regions, but noted that while these attributes point to high-frequency energy reduction, there is no one-to-one correlation between attenuation and gas presence since reservoirs are largely complex. These statistical attributes Li et al. (2015, 2016) applied are called “shape attributes” and measure the shape of the seismic amplitude spectrum. Although these spectral attributes have not previously been

applied to measure attenuation within hydrates, instantaneous and amplitude versus offset (AVO) attributes have proven useful for evaluation of gas hydrate-bearing sediment (Wang et al. 2023; Clairmont et al. 2021). Instantaneous attributes are incorporated with skewness and kurtosis into unsupervised machine learning to further identify gas hydrates in seismic data in the absence of BSRs or other clear direct hydrocarbon indicators (DHIs).

The goal of this study is to (1) determine whether or not skewness and kurtosis are useful attributes for measuring attenuation related to gas hydrate accumulation in the GHSZ and can therefore serve as hydrate indicators and (2) implement unsupervised machine learning based on spectral, amplitude and frequency-related attributes to enhance attenuation-related responses and variations visible in the selected attributes.

Physical characteristics of gas hydrates

Gas hydrates, chemically described as clathrate hydrates, were first discovered in 1810 by Sir Humphry Davy, but their significance was disregarded until the early decades of the 20th century when hydrates were recognized as an engineering concern due to well-bore plugging within the oil and gas industry (Hammerschmidt 1934; Englezos, 1993; Riedel et al. 2010). Hydrogen-bonded water molecules form the lattice of the clathrate structure, in which the “guest” or methane molecule is enclosed (Englezos, 1993). The configuration of the chemical lattice can vary across three main structures (I, II and H) of clathrates, with a simple methane hydrate classified as type I (Riedel et al. 2010).

In-situ, methane hydrates have similar physical properties to ice and behave as a solid. Hydrates increase the rigidity of strata, while reducing porosity due to the pore-filling nature of hydrates (Riedel et al. 2010; Dvorkin et al. 2014). Two separate models for hydrate occurrence within sediment pore space were described by Dvorkin et al. (2014) and constitute (1) hydrates existing within the *mineral frame* of the pore space and (2) hydrates existing in the pore fluid of the pore space. Observations from numerous studies show that both P and S-wave velocities are impacted by gas hydrates, although often at different scales (Best et al. 2010), pointing to the likelihood of hydrates within the mineral frame of the rocks (Dvorkin and Mavko 2006; Guerin and Goldberg, 2002; Liu et al. 2022). Whichever model is applied, the reduction in porosity and increase in frame rigidity due to hydrates leads to the increase in both elastic moduli and subsequently, velocity (Dvorkin et al. 2014), and the opposite effect of decrease in velocity observed at the base GHSZ/ below the BSR due to free gas accumulation (Singh et al. 1993).

Seismic attenuation associated with gas hydrates

Attenuation is energy loss exhibited in the seismic signal, and is denoted by the quality factor, Q , which is inverse attenuation (Riedel et al. 2010). Attenuation is expected to result in a reduction of higher-frequencies over low-frequencies (Raikes and White 1984), and there is evidence of a low-velocity shadow zone (LVSZ) below high attenuation zones associated with hydrates (Taylor et al. 2000) and other types of gas accumulations (Castagna et al. 2003) trapped below the GHSZ. Although there are several mechanisms proposed for attenuation, the exact nature of attenuation within hydrates is not yet fully realized since the attenuation responses have proven to be complex (Dvorkin et al. 2014; Riedel et al. 2010) and lacking a clear one-to-one correlation between hydrate saturation and attenuation (Liu et al. 2022). Furthermore, while one might expect lower attenuation in stiffer, more dense, or low-porosity rock (Klimentos and McCann 1990), the opposite effect of increasing attenuation with hydrate saturation is overwhelmingly observed (Guerin and Goldberg 2002; Chand and Minshull 2004; Dvorkin and Uden 2004; Riedel et al. 2010, and references therein; Dvorkin et al. 2014 and references therein; Zhan and Matsushima 2018; Sahoo et al. 2019), to the extent that some researchers advocate for attenuation to be considered within the realm of physics-driven seismic attributes for both conventional and unconventional reservoir characterization (Dvorkin and Mavko 2006) and methane hydrate reservoir characterization (Cordon et al. 2006).

One study that constructed a set of synthetic seismic data based on properties in the Mallik 2 L-38 well drilled in the Mackenzie Delta, Canada, applied an inverse Q (Q^{-1}) parameter to synthetic seismic and showed that higher frequencies (50 Hz) exhibited greater reduction in amplitude than did lower frequencies (20 and 30 Hz) when compared to the same synthetic seismic with no Q^{-1} factor applied (Cordon et al. 2006). Another study showed that any hydrate saturation resulted in increased attenuation (up to a point determined by frequency) seen in the P-wave velocity measured from cross hole tomography and sonic logging (Chand and Minshull 2004). Yet another showed that even low hydrate saturation resulted in amplitude losses while simultaneously increasing both compressional and shear velocities due to stiffening of the pore space (Guerin and Goldberg, 2002). Attenuation mechanisms that have been applied to hydrate studies include the patchy saturation mechanism (first proposed by White 1975, and applied in a study by Liu et al. 2022), the macroscopic fluid flow mechanism (first proposed by Biot 1956a, b, and applied by Cordon et al. 2006), and a combined Biot–Squirt flow mechanism (applied by Chand and Minshull, 2004). The numerous hydrate studies and attenuation responses illustrate the complex nature of attenuation. Attenuation effects from hydrates should be

observable in seismic or well data and related frequency spectra. Based on the current understanding of attenuation in hydrates, observing increased attenuation due to known presence of gas hydrates in the Pegasus Basin is a primary objective of this study.

Attribute and attenuation variation with angle

A unique aspect of this project is that it gives the opportunity to study how attenuation effects may be seen at different angles in the seismic reflection data. While this is not strictly an amplitude variation with offset (AVO) or angle (AVA), there are expected variations between a full stack, near angle stack, or far angle stack. The frequency content is expected to vary from the far to near angle stacks; while there is naturally occurring attenuation in the far angle stacks as the seismic wave travels further through the earth to those angle location, there may also be impacts from normal move-out (NMO) corrections resulting in reduced frequency in the far angle stacks (Hilterman and Van Schuyver 2003). This may impact skewness and kurtosis attribute responses across the different angle ranges, as the frequency spectrum will subsequently be impacted by the degree of attenuation of the seismic frequencies.

Geologic setting of the Pegasus Basin

Structural setting and Basin history

The Pegasus Basin is a triangular-shaped basin located offshore New Zealand between the North Island and the Chatham Rise (Bland et al. 2015; see Fig. 1), and is synonymous with the Southern Hikurangi Trough Margin (see map). The Pegasus Basin sits adjacent to an area characterized by a series of NE–SW trending reverse and strike-slip faulting along the western edge of the basin which represent the convergence of and subduction zone between the Pacific plate to the northeast and the Australian plate to the southwest (DeMets et al. 2010). Along the North Island, the Hikurangi Trough serves as the boundary between the subducting Pacific plate, forming a thrust fault as the Pacific plate subducts below the North Island, while to the southwest, the Alpine Fault comprises a series of left-lateral strike-slip faults along the plate boundary which cuts across the northern South Island and then parallels the western extent of the island. Along the southern border of the Hikurangi Trough is the Chatham Rise, an east-west linear bathymetric feature that is remnant from the once-active eastern margin of Gondwana (Bland et al. 2015; King 2017). Primary clastic sedimentation in the basin resulted from deposition from the Hikurangi Channel, sourced by sediments from the Southern Alps (Lewis

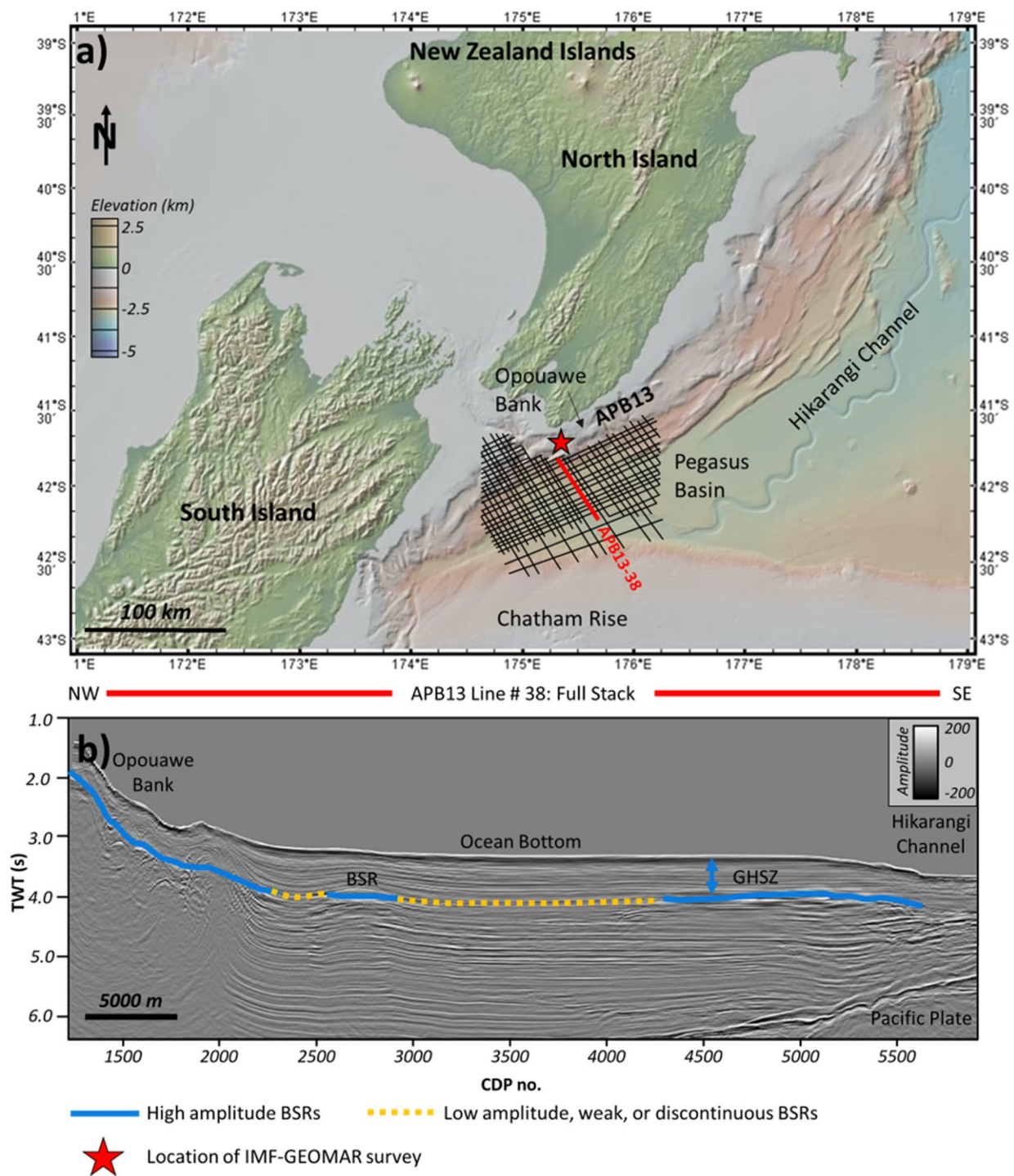


Fig. 1 a Map of the Pegasus Basin and APB13 2D seismic volume, and b ABP13 line # 38 in TWT (two-way time) with high and low amplitude BSRs. Refer to Fig. 4 for uninterpreted BSRs across the study area. Bathymetric basemap taken from GeoMapApp

et al. 1998). Overall, the Pegasus Basin covers an area of approximately $\sim 25,000 \text{ km}^2$, although the eastern extent of the basin is poorly constrained by seismic data and could be much larger than the previously mentioned area. While the deepest part of the Pegasus Basin is over 3000 m below

sea level (mbsl) in the northeastern end, the average depth is $\sim 1000\text{--}1500 \text{ mbsl}$ (Bland et al. 2015; See Fig. 1). The broad vertical and horizontal occurrence of hydrates over a subduction zone with thermogenic and biogenic methane

sources (Kroeger et al. 2015) make this an excellent basin to study the seismic expression of hydrates.

Stratigraphy

Within the Pegasus Basin, the stratigraphy is considerably enigmatic since there is no well control in the basin, with the closest well 150–200 km away in the East Coast Basin, located to the northwest of the Hikurangi Trough. Nevertheless, seismic data acquired over the past few decades, as well as bathymetry and core (gravity and piston) data have proven useful to interpretations of the stratigraphy throughout the Pegasus Basin. The focus of this paper is on the shallow succession of primarily Neogene trench fill within the basin, is predominately interpreted as mixed siliciclastics (mudstone, siltstone, and sandstone) from turbidite deposits (Lewis and Pantin 2002) or seafloor current deposits (Kroeger et al. 2015, and references therein), with evidence of sediment waves and levee deposits in relation to the paleo-Hikurangi Channel (Lewis and Pantin 2002). Collier (2015) tied Cretaceous-Neogene outcrops onshore New Zealand to seismic data from the PEG09 2D seismic survey and determined that in the late Neogene, sedimentation rates were high and resulted in thick sediment packages in the basin. From the seismic, the deeper trench-fill Miocene deposits are interpreted as flysch deposits based on their seismic response (continuous, high-frequency reflectors) and a “cut and fill” geometry that indicates coarse-grained channel deposits (Collier 2015).

Previous gas hydrate studies in the Pegasus Basin

Hydrates have been recovered along the Opouawe Bank in the Pegasus Basin by the IMG-GEOMAR NEMESYS cruise in 2011 which sought to map the extent of the active methane seepage along the Hikurangi Margin (Bialas 2011; see map inset in Fig. 4). In addition deeply-occurring hydrates throughout the Neogene, hydrates have also been recovered from gravity cores in the Hikurangi subduction margin (Plaza-Faverola et al. 2012). A recent study conducted over the Pegasus Basin showed that a combination of seismic attributes (instantaneous frequency, sweetness, thin bed, fluid factor, and gas indicator) and unsupervised machine learning (self-organizing maps) can help detect weak and discontinuous BSRs (Chenin and Bedle 2020). Another study (Clairmont et al. 2021) over the Pegasus Basin used primarily frequency attributes (instantaneous frequency and sweetness) and spectral decomposition to resolve weak BSRs, and sparse-spike decomposition to estimate the quality factor, Q , which is the inverse of attenuation. The results showed that the frequency-related attributes helped identify free-gas zones (FGZ) below the BSRs and the spectral decomposition helped differentiate the low-frequency

shadow zones and BSRs from the background seismic. The Q -estimation gave provided additional support for gas accumulation below the identifiable, high amplitude BSRs. Finally, a recent study by Wang et al. (2023) used attenuation and stratigraphic attributes to analyze attenuation throughout the Hikurangi and Hikurangi Trough.

While many studies rely on the BSR as a primary indicator of gas hydrates and have even shown that BSRs can be enhanced through careful seismic attribute selection and machine learning, there are few studies that attempt to detect gas hydrates from attenuation alone. Hydrates can exist in systems that lack a clear BSR (e.g. Majumdar et al. 2016), and when well data is unavailable, quantifying attenuation through seismic attributes may prove to be the most compelling evidence of hydrates, in addition to being a straightforward and cost-effective alternative to acquiring well or core data. The presence of high amplitude BSRs in conjunction with low amplitude, weak and or discontinuous BSRs seen in seismic data, as well as core reports indicating the presence of hydrates in the shallow subsurface toward the western edge of the basin, makes the Pegasus Basin a valuable study area to delineate the statistical attributes’ ability to quantify attenuation across a variety of geophysical expressions of hydrates, while in a relative lithological homogeneity.

Available data

The APB13 dataset, acquired in 2014, data was processed by CGG Services (Singapore) Pte Ltd in 2014 using a full Kirchhoff pre-stack time migration (PTSM) and a post-stack processing utilizing Q -compensation and time variant scaling (New Zealand Petroleum & Minerals Report PR5170). The seismic data is normal SEG polarity with the ocean bottom being a strong peak seismic reflector (Table 1).

In addition to the full stack data, the near (NAS), mid (MAS) and far (FAS) angle stacks are also available and while the middle angle stacks are available, for this research,

Table 1 Survey parameters for the APB13 seismic survey. From New Zealand Petroleum & Minerals Report PR5169 (2014)

No. 2D lines	56
No. channels	648
Record length	10,500 ms
Streamer length	8100 m
Sample rate	2 ms
Shot point (SP) interval	37.5 m
Source capacity	3610 cu in
Angle stacks	Range
Near (NAS)	5–18°
Mid (MAS)	18–32°
Far (FAS)	32–45°
Full	40° inner/outer mute

they were not utilized as there is not expected to be a significant response due to angle offset seen in the middle angles.

Although there is no available well data in the Pegasus Basin, the presence of gas hydrates has been confirmed by seafloor cores (see map inset in Fig. 4; Bialas 2011; Plaza-Faverola et al. 2012 from the IMF-GEOMAR cruise in 2011 and indicators of gas hydrates -in the form of BSRs - can be clearly seen in the seismic amplitude data, making the APB13 seismic survey a valuable asset in determining attenuation through hydrates.

Methods

Data conditioning

The methodology for this study, as outlined in Fig. 2, begins with the seismic amplitude volume. Care must be taken at the beginning to determine whether or not the seismic amplitude has been previously spectrally-balanced during the processing stage. It is expected that spectrally balancing the data, while improving the vertical resolution and preconditioning the data for subsequent spectral analysis, would undermine the accuracy of specific spectral shape attributes which measure the asymmetry of the seismic amplitude spectrum. While spectrally-balanced data may be used for other attribute calculations, for consistency within this study, only non-balanced data was used for all the attribute calculations.

APB-13 seismic line #38 was chosen for attribute and machine learning implementation due to the proximity to previous studies on the APB13 and PEG09 seismic surveys (see Chenin and Bedle 2020, and Clairmont et al. 2021) The seismic line was subdivided into five zones with distinct

seismic characteristics and attribute variations in order to better characterized the attribute results in a later section. The zones (Fig. 4c) correspond to the following approximate depth or seismic feature cutoffs throughout the GHSZ: Ocean bottom (Zone 1), immediately below ocean bottom reflector to 3.53 s (Zone 2), 3.54–3.79 s (Zone 3), 3.8 – BSR (Zone 4), BSR (Zone 5).

Spectral decomposition

After picking the major stratigraphic reflectors of interest and/or cropping the seismic amplitude volume, a spectral decomposition method based on the continuous wavelet transform (CWT) is used to decompose the seismic into its frequency components. Grossmann and Morelet (1984) first define the CWT as a cross-correlation between the seismic trace and a dilated version of a basic wavelet, which allows the CWT results to include information about the time/depth and frequency of the seismic trace. The continuous wavelet transform has been used for many applications in geophysics, from (1) improving seismic resolution for reservoir geometry studies (Matos et al. 2012) to (2) application of spectral components (computed from CWT) for resolving subtle stratigraphic features in carbonate and clastic reservoirs (Davogustto et al. 2013) and (3) improving vertical imaging within 3D seismic datasets (Peyton et al. 1998). In this research, the spectral decomposition is necessary to decompose the seismic into its spectral components; this allows the algorithm to compute the statistics (i.e., skewness and kurtosis), on the frequency spectrum across each sample (rather than by trace, line, or volume). Therefore, the statistical response is calculated from the spectrum at each individual point or sample in the data, rather than across the entire seismic line or cropped volume.

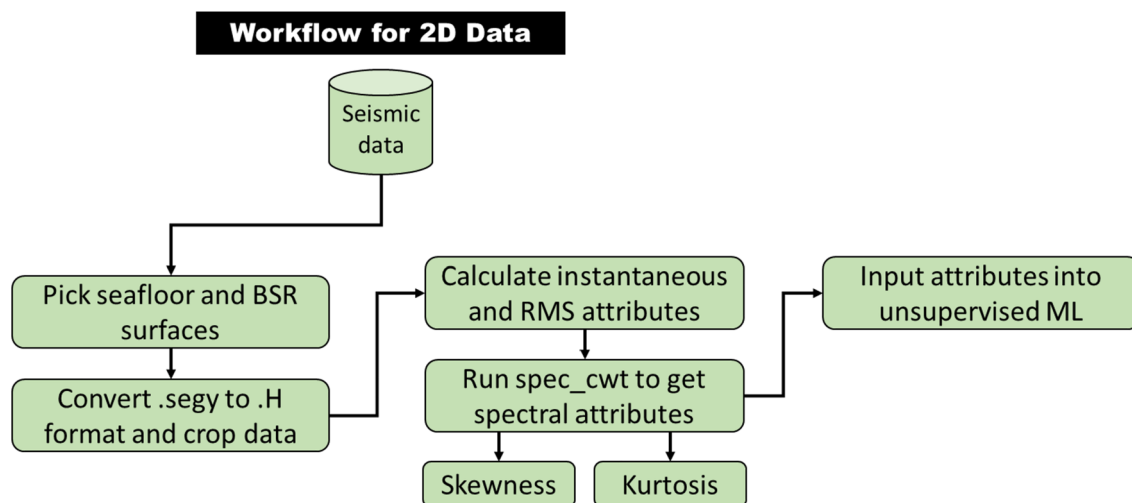


Fig. 2 Project methodology and workflow for seismic data handling, attribute calculation, and machine learning implementation

Seismic attributes

As the focus of the study is to identify the attenuation in the seismic due to gas hydrate presence, seismic attributes that are related to frequency were chosen as they best detect attenuation of the seismic waveform. Among these, spectral skewness and kurtosis attributes represent the frequency spectrum of the seismic amplitude volume computed using a continuous wavelet transform. These attributes are implemented through a spectral attributes utility which is a spectral decomposition method based on the continuous wavelet transform, as discussed previously.

Spectral skewness attribute

Skewness is a statistical measure that defines how much a dataset deviates from the mean of the data (Fig. 3). It is the 3rd moment of the standard score of the variable Y (seen in the equation below, Eq. 1). Data that is skewed toward the left has positive skewness, data that is skewed toward the right has negative skewness, and data that is perfectly symmetric around the mean has 0 skewness. Skewness has been used for seismic analysis before as seen by Li et al. (2016) to characterize attenuation within conventional and unconventional hydrocarbon reservoirs, and is given by the equation.

$$Skewness = \frac{\sum_i^n (Y_i - Y)^3}{(n - 1)\sigma^3} \tag{1}$$

where σ is the standard deviation of the dataset and Y is the random variable to be defined, or in this case, amplitude. In

this study, skewness is applied as an attribute to measure attenuation seen in the frequency spectrum of the seismic data. Since it has been shown that hydrates often attenuate high frequencies over low frequencies (Raikes and White 1984), attenuation of high frequencies is expected to give a positive skewness response as the data becomes skewed toward the low-frequency end of the spectrum (Fig. 3a, see positive skewness example). However, one consideration is that these metrics are in comparison to a normal or Gaussian distribution of data, and it is important to note that seismic data is inherently non-Gaussian. A typical seismic spectrum is expected to be overall positively skewed due to seismic data containing generally a higher percentage of low frequency to high frequency as the earth is a natural attenuator.

Spectral kurtosis attribute

Kurtosis is a statistical measure that defines the “tailedness” of, or the distance of the tails from the mean in a normal distribution (Fig. 3b) of a dataset. It is the 4th moment of the standard score of the variable Y (as seen in Eq. 2 below). Although kurtosis is always positive and ranges from 1 to infinity, “excess positive” refers to data that is heavily-tailed and has a large amount of outliers, also referred to as *leptokurtic*. “Excess negative” describes data that is light-tailed and has very few outliers, sometimes referred to as *platykurtic*. A normal distribution of data will have a kurtosis value of 3, so normalizing the data about 3 gives excess negative kurtosis at a value of -2 and while excess positive is a value of +2 (Sharma 2020). Kurtosis was also applied by Li et al. (2016) and is given by the equation.

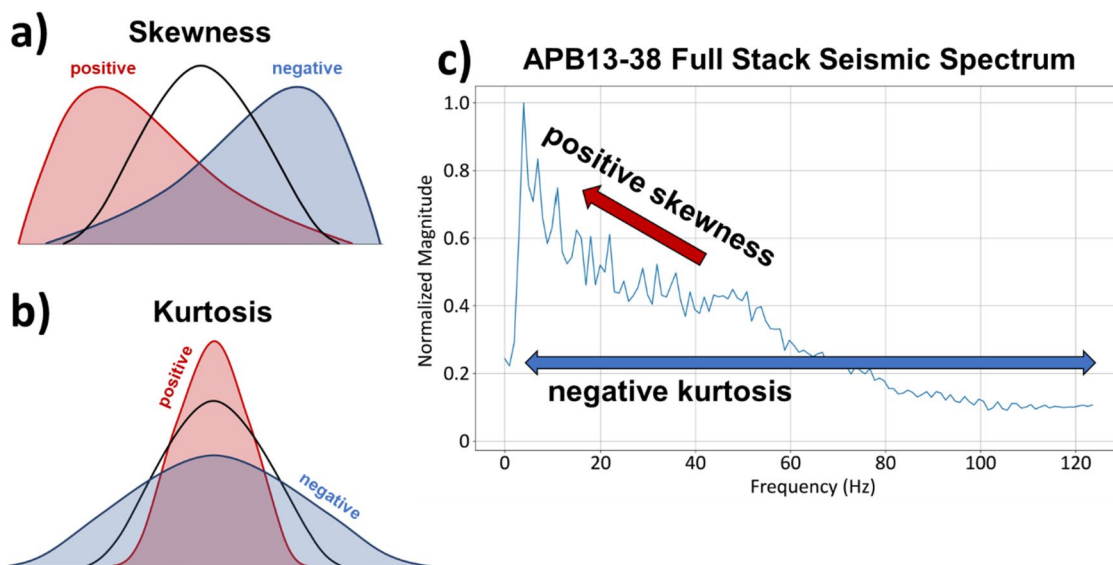


Fig. 3 a Skewness variations with positive (red line), negative (blue curve), and normal (black curve) skewness, b Kurtosis with positive (red curve), negative (blue curve), and normal (black curve) kurtosis,

and c Amplitude spectrum from APB-13 seismic survey line #38 showing overall positive skewness and negative kurtosis

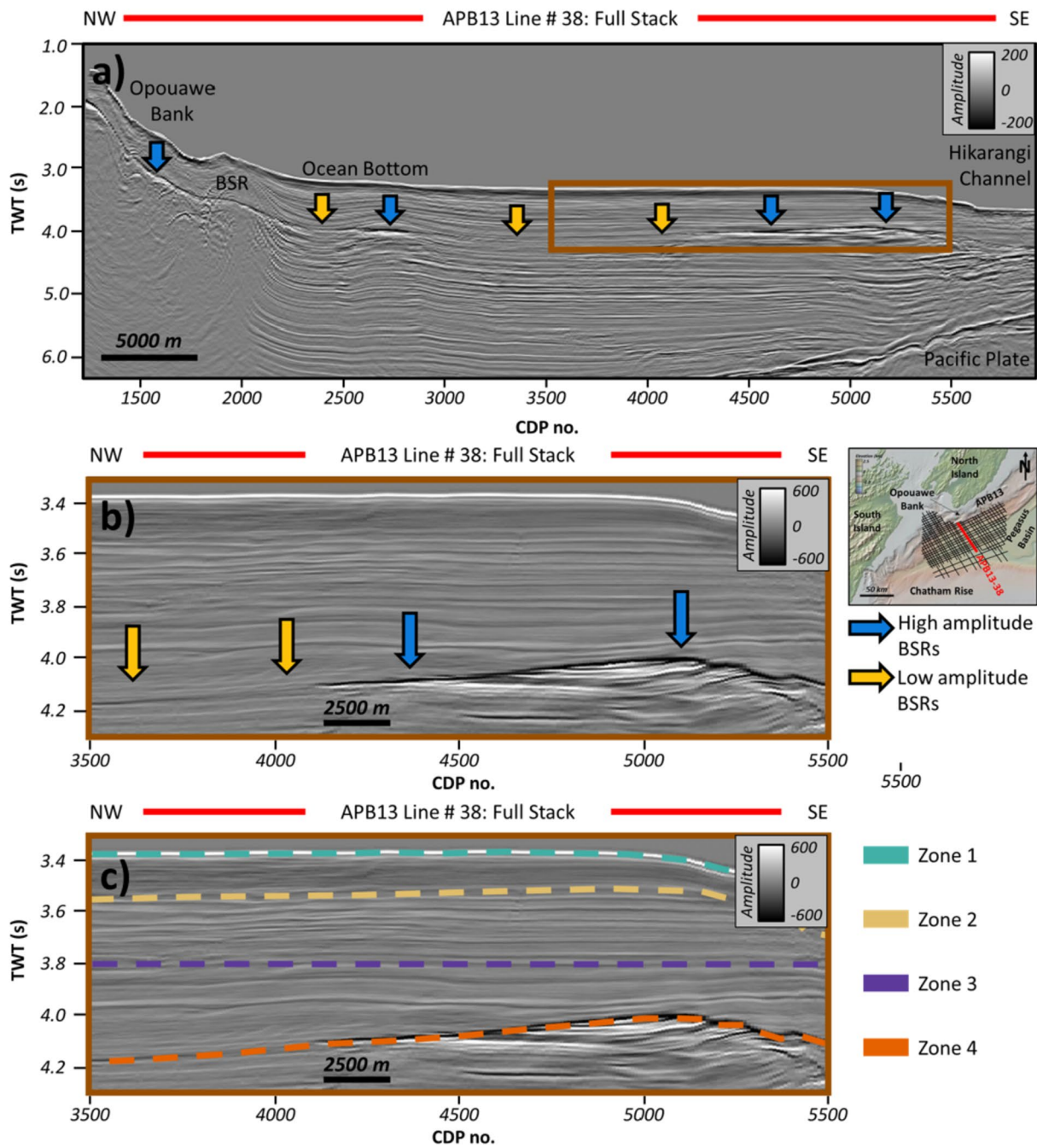


Fig. 4 a Full stack seismic line across the Pegasus Basin, b Interpreted areas showing BSR extent (both high and low amplitude) throughout the seismic line, and c Attribute variations zones 1–4; seafloor bathymetry map from GeoMapApp

$$Kurtosis = \frac{\sum_i^n (Y_i - \bar{Y})^{-4}}{(\sum_i^n (Y_i - \bar{Y})^2)^2} \quad (2)$$

A lower peak frequency, as demonstrated by Li et al. (2015) is expected to present as positive kurtosis. Positive kurtosis may also be thought of in relationship to bandwidth; a narrower bandwidth from attenuated frequencies

should therefore exhibit positive kurtosis. Kurtosis is often casually described in terms of the “peaked-ness” of a dataset, with negative kurtosis being low-peaked and positive kurtosis being high-peaked. While these descriptions may be useful for understanding the shape of a spectrum in some circumstances, it is more accurate to describe kurtosis in relationship to the outliers, i.e., tails.

RMS Amplitude Attribute

Root mean square (RMS) amplitude is a commonly applied seismic attribute that is computed such that the root-mean-square of the data, $d(t)$, is given by:

$$d_{RMS}(j\Delta t) \equiv \sigma(j\Delta t) = \left(\frac{1}{2K+1} \sum_{k=-K}^{+K} \{d[(j+k)\Delta t]\}^2 \right)^{1/2} \quad (3)$$

and calculated over a user-defined analysis window (Chopra and Marfurt 2007) with range equal to $-T = K\Delta t$ to $+T = +K\Delta t$. RMS amplitude is applied to this study as it is a good indicator of changes in amplitude and can be contrasted with the frequency attributes to determine whether attenuation response is tied to amplitude or frequency variations across the GHSZ and how those relate to the geology and stratigraphic nature within the Pegasus Basin.

Envelope attribute

Envelope, also called the instantaneous amplitude attribute or reflection strength, is a complex trace attribute that was described by Taner et al. (1979) as related to a reflection event along the seismic trace and is calculated from the seismic trace ($u(t)$) and the Hilbert transform [$u^H(t)$] such that.

$$e(t) = \left\{ [u(t)]^2 + [u^H(t)]^2 \right\}^{1/2} \quad (4)$$

Envelope is useful as a thin-bed tuning indicator and also can be used to represent changes in lithology, porosity and hydrocarbon accumulation due to its relationship to acoustic impedance contrast (Chopra and Marfurt 2007). For this study, envelope is useful for enhancing the BSR related to gas hydrate accumulation and for determining non-frequency-related responses in a hydrate system. Additionally, envelope is one of the parameters used to calculate the sweetness attribute, which is described in Sect. 3.3.6.

Instantaneous frequency attribute

The instantaneous frequency attribute is calculated as the derivative of the instantaneous phase attribute by the equation (Eq. 3).

$$f(t) = 2\pi \frac{d\phi(t)}{dt} \quad (5)$$

where $\phi(t)$ is the instantaneous phase and $f(t)$ is the seismic trace. Instantaneous frequency is commonly used for thin-bed tuning and, since it is a frequency-derived attribute, can also give clues about attenuation (Chopra and Marfurt 2007). Instantaneous attributes such as instantaneous frequency and envelope (described below) have been applied

in the Pegasus Basin by other authors (Fraser et al. 2016) and were found to be useful for highlighting attenuation response (Clairmont et al. 2021) and for detecting weak BSRs (Chenin and Bedle 2020). In this study, instantaneous frequency is used in addition to skewness and kurtosis to give feedback about the attenuation response and how hydrates impact the frequency spectra of the seismic data.

Sweetness attribute

Sweetness is another commonly-used attribute for hydrocarbon settings and enhancing low frequency, high amplitude zones that may be representative of hydrocarbon-filled sands. Sweetness is calculated from the instantaneous frequency and envelope attribute, so it gives a unique combination of both frequency and amplitude responses:

$$s(t) = \frac{e_{resp}(t)}{[f_{resp}(t)]^{1/2}} \quad (6)$$

where e is the envelope of the seismic trace and f is the frequency of the seismic trace. For this study, sweetness is useful for channel detection, highlighting clean sand layers (Hart 2008), and subtle changes in amplitude and frequency, the latter of which is especially useful for measuring attenuation.

Unsupervised machine learning - SOMs methodology

Self-organizing maps theory and previous hydrate applications

At its basic level, self organizing maps (SOMs) are a pattern-recognition method of machine learning based on theory that allows the algorithm to take input data (in this case, seismic attributes) and group that data into “feature maps” that can be tied to some meaningful geological or geophysical relationship (Kohonen 1982, 1990). The mapping process takes N-dimensions of data (set by the number of input attributes), determines how those J-vectors comprising the attributes are related to each other within the latent space, and projects the output vectors into a lower-dimensional space or “manifold” in which space the algorithm can form clusters (Zhao et al. 2015, 2018), also called neurons, “prototype vectors,” or SOM units (AASPI som3d program documentation, 2020). These neurons or vectors are then colored by a 2D color bar that has the number of classes determined during the input parameters (discussed below) and the SOM implementation.

SOMs have been applied in other seismic studies to interpret deep-water seismic facies and architectural elements (La Marca and Bedle 2021; La Marca et al. 2019) and characterize turbidites in seismic data (Zhao et al.

2016), and to evaluate reservoir lithology and rock type changes (Hussein et al. 2021). SOMs have also been used to enhance weak or discontinuous BSRs (Chenin and Bedle 2020), and combined with PCA to discriminate BSRs from surrounding lithology (Lubo-Robles et al. 2023). It's important to note that when applying SOMs to a particular research problem, the input attributes should be appropriate to the specific research goal; that is, geometric attributes should be used to answer questions about the structure or stratigraphy of a seismic dataset (Zhao et al. 2018), or spectral shape attributes to measure attenuation of the amplitude spectrum, and so forth.

Self-organizing maps implementation

In total, the six attributes (spectral skewness, spectral kurtosis, instantaneous frequency, envelope, sweetness, and RMS amplitude) were input into the SOM algorithm, and each attribute was normalized using a z-score algorithm. The maximum number of classes for each SOM case was set to 256 as this is the maximum number many software can visualize, although the algorithm determines the final (if smaller than 256) number of classes (AASPI som3d documentation, 2020). The number of data training iterations was set to 30, and the crossline (CDP) decimation in training, line decimation in training, and vertical sample decimation in training were all set to 2 as this value was considered a robust decimation rate for the dataset. Larger decimation values of 5 were initially tested, however, these were not fine enough to resolve all the pixels within the data. The SOM was implemented across a window defined by a top (ocean bottom) and base (BSR) horizon. The horizons were mapped and gridded from the 2D seismic lines (for each of the full, far, and near angle stacks) in a separate seismic interpretation software. The outputs are two SOM projection axes (Projection Axis 1 and Projection Axis 2). The final SOM output or facies map is created by cross-plotting the two projection axes against each other. The SOM facies are colored based on a 2D color map, which is generated from the number of classes determined during input and by the algorithm and co-rendered with the histogram of clusters that occur in the data.

Results

The results for the spectral shape and supplemental attributes and unsupervised machine learning are presented below. Careful descriptions are given to aid understanding of how attribute response is related to attribute theory.

Seismic amplitude volume description

In the APB-13 survey across the Pegasus Basin, the ocean bottom occurs as a strong peak reflector [average approximately 700 dB across the full stack seismic cropped window in Fig. 1b] that is easily identifiable in the seismic data (see Fig. 1). The BSR roughly mimics the ocean bottom reflector's absolute strength, with opposite polarity. In the seismic data, the BSR appears from 2 to 5 s two way time (TWT), ranging from the northwest along Opouawe Bank to the southeast across the Hikurangi Channel. Across these regions, the BSR is a continuous, medium to high amplitude trough (Figs. 6 and 7). Chenin and Bedle (2020) and Clairmont et al. (2021) interpret discontinuous BSRs that extend throughout the central part of the Pegasus Basin (between 3000 and 4500 CDP on ABP13 line 38) and more continuous BSRs that extend upward along the Opouawe Bank to the northwest and from CDP 4500 to the edge of the seismic survey in the Hikurangi Channel (Figs. 6 and 7). The BSR is most easily identified where it crosscuts structure and stratigraphy along the flank of the Opouawe Bank and the southeast edge of the survey. These areas present high amplitude BSRs and are associated with microbial methane accumulations (Kroeger et al. 2015) and high Q^{-1} (inverse quality factor or attenuation) values below, and in some cases, above, the BSR (Clairmont and Bedle, 2021). Since it is already known that hydrates do occur in this area of the Pegasus Basin, now the aim of the project is to build on the previous work to measure the attenuation *within* the GHSZ instead of below the BSR.

Using the BSR as an indicator of the approximate BGHSZ, attenuation is expected to occur anywhere within the GHSZ where hydrate accumulation occurs. To limit the area of focus to exclusively the hydrates within the GHSZ, a smaller cropped interval (roughly between 3.3 and 4.3 s TWT and between CDP numbers 3500–5500) was analyzed (Fig. 4b). This area contains high amplitude BSRs [ranging between -400 to -700 dB (55% and greater absolute strength of the seafloor reflector) between CDP 4100–5500] in addition to low amplitude [ranging between -80 to -200 dB (10–25% absolute strength of the seafloor reflector) between CDP 3500–4100] BSRs, providing an opportunity to study attenuation in the presence *and* absence of BSRs, and determine if attribute response may vary throughout the GHSZ with or without a BSR. Within this cropped interval of data, the BSR exhibits as a high amplitude seismic reflector, sub-parallel to the ocean bottom toward the western edge of the Hikurangi Channel, and transitions to low amplitude toward the central section of the basin (Hikurangi Trough). The seismic reflectors throughout the seismic line (Fig. 4b and corresponding attribute figures) are horizontal to sub-horizontal, parallel and fairly continuous; however, between 3.53 and 3.8 s TWT, there is a series of increased absolute

amplitude (compared to the background, non-seafloor or BSR) [absolute amplitude ~ 150–275 dB], thin [~ 20 ms TWT, especially concentrated between CDP 3800–4500], sub-parallel reflectors (see Fig. 4b and c) that exhibit absolute amplitude increase with angle and that may represent sediment waves described by Lewis and Pantin (2002).

Attribute volumes

Seismic attribute analysis was performed on each of the statistical attributes and on the five supplemental frequency-, trace-, and amplitude-related attributes prior to implementing the machine learning. This was done to assess whether the attributes could contribute to enhancing variations in the GHSZ due to attenuation from hydrate accumulation. While the main focus is the statistical attributes, as they are novel and untested in this approach and the four

supplemental attributes are already proven to be applicable in a hydrocarbon setting, all the attributes were carefully inspected. Results were characterized from the ocean bottom to the base of the gas hydrate stability zone to determine each individual attribute’s contribution to understanding the hydrate system. Furthermore, the combination of frequency and amplitude-related attributes provides a robust suite of attributes for the SOM implementation in the machine learning phase (Fig. 5).

Spectral skewness attribute

With respect to the variations across the angle stacks described below: while the skewness variation is not strictly an AVO-type response, since it’s not the amplitude of the seismic that is being analyzed, the amplitude of the skewness

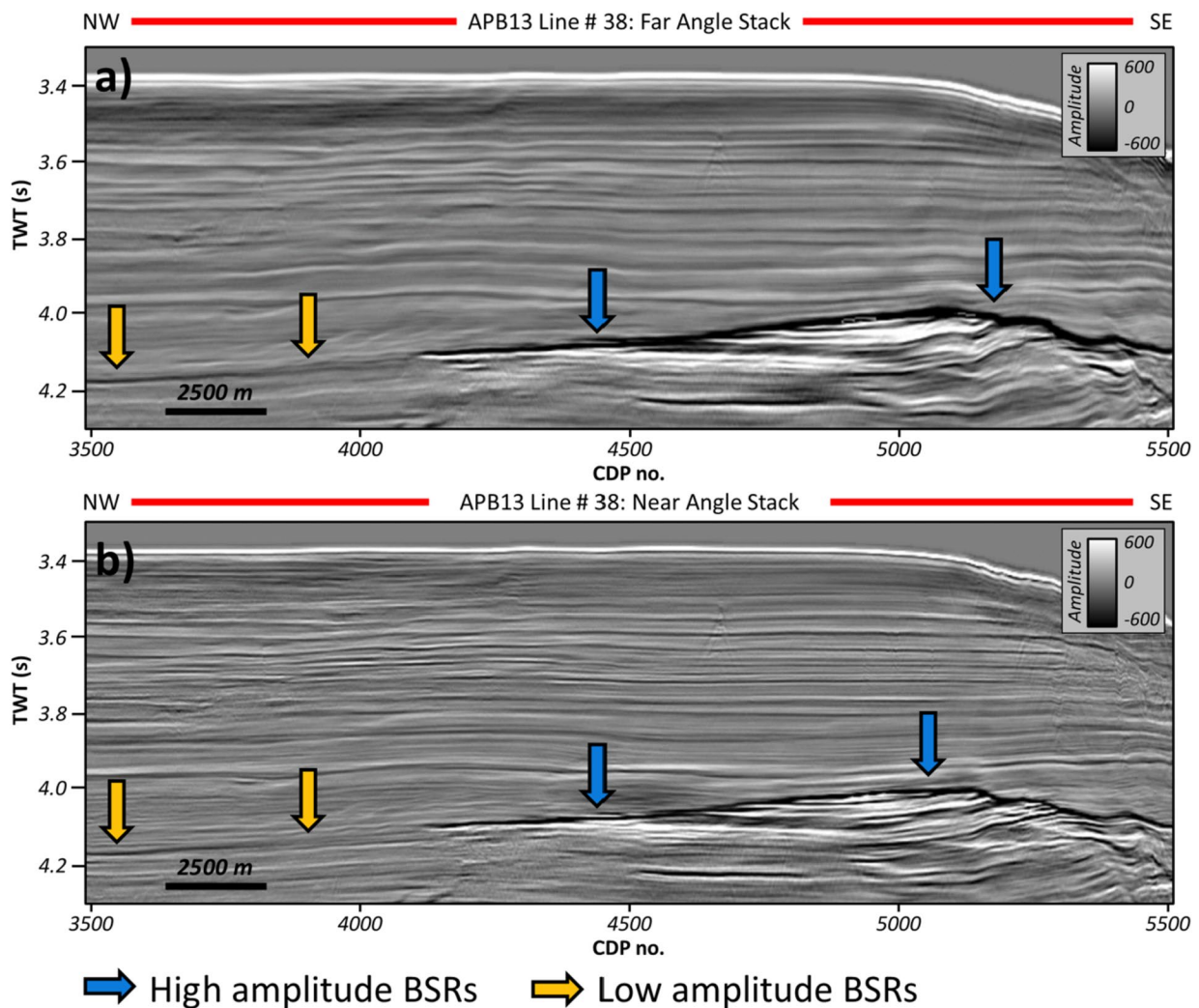


Fig. 5 a Far angle stack seismic line with high and low amplitude BSRs, and b Near angle stack with high and low amplitude BSRs; the seismic amplitudes are plotted on the same scale for each of the full, far, and near angle stacks. See Fig. 4 for seismic line map locations

Fig. 6 **a** Full stack seismic line with high and low amplitude BSRs and Zones denoted by color, **b** Skewness attribute calculated from the full stack seismic line, **c** Full stack amplitude co-rendered with full stack skewness, **d** Skewness attribute calculated from the far angle stack seismic line, and **e** Skewness attribute calculated from the near angle stack seismic line. See Fig. 4 for seismic line map locations

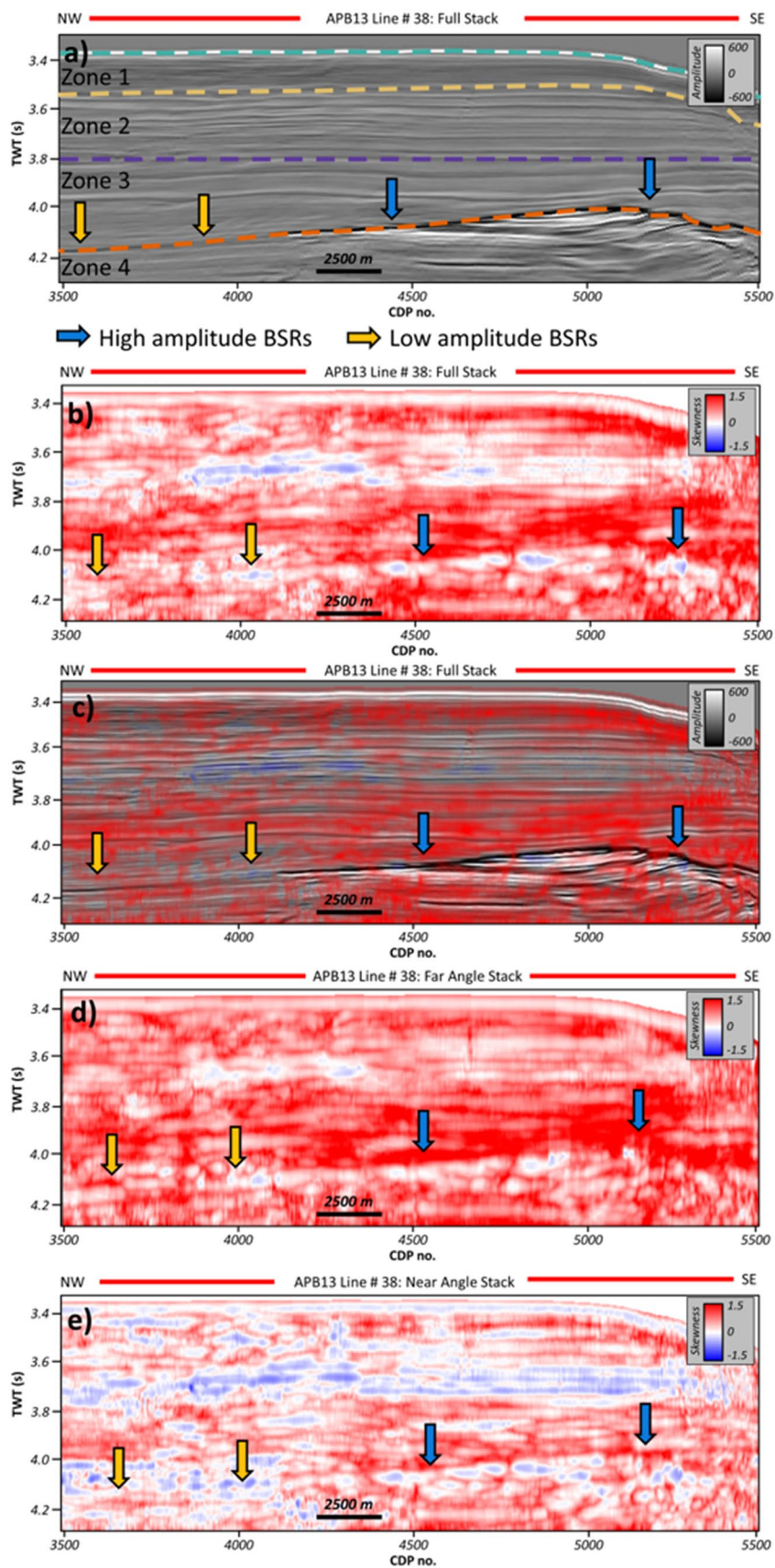
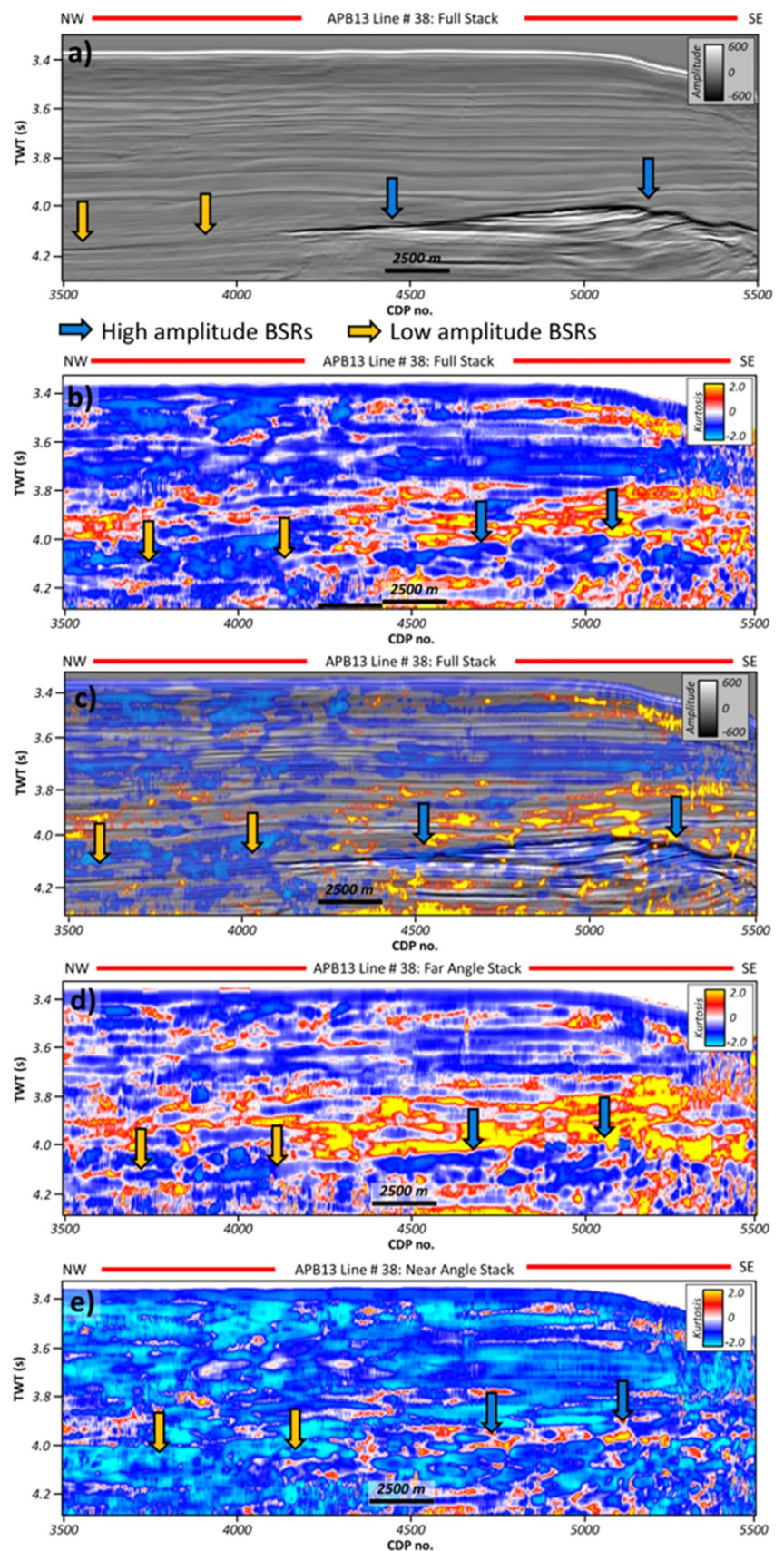


Fig. 7 **a** Full stack seismic line with high and low amplitude BSRs and Zones denoted by color, **b** Kurtosis attribute calculated from the full stack seismic line, **c** Amplitude co-rendered with kurtosis attribute, **d** Kurtosis attribute calculated from the far angle stack seismic line, and **e** Kurtosis attribute calculated from the near angle stack seismic line **e** See Fig. 4 for seismic line map locations



response is varying with angle, therefore, the term “skew-AVO” was coined to describe the effect.

Throughout the GHSZ in Zone 1, is generally positive, ranging from 0 to 1.5 (Fig. 6a and b). Higher skewness values [~ 1.4 to 1.8] are observed in the SW along the Hikurangi Channel slope, from CDP 5000–5400. The skewness of the ocean bottom is low, usually less than 0.1 across the window. In Zone 2, skewness is a mix of positive and negative, with negative skewness [-0.3 to -0.6] dominating throughout CDP 3850–4450 and varies across the entire Zone 2. The negative skewness band is seen most clearly in the full stack and near angle stack attribute lines, while it is less continuous and plots closer to 0 skewness in the far angle stack. The negative skewness described in Zone 2 roughly corresponds to the thin-bedded, sub-parallel reflectors described in the seismic amplitude line Zone 2.

In Zone 3, skewness is again generally positive, ranging from 0 to 1.5 (Fig. 6a and b). Skewness is highest [1 to 1.6] between CDP 4300–5500, immediately above the high amplitude BSR. The strongest skewness response [especially above the strong BSR in CDP 4300–5500, skewness is as great as 2.2 in places] is observed in the far angle stack, although it is comparable to the full stack line’s skewness response, with noticeably weaker positive skewness [0.8 to 1.4 in the same location mentioned previously] in the near angle stack. The near angle stack also contains larger patches of slightly negative skewness [-0.3 to -0.5] directly above the *weak* BSR toward the northwest end of the seismic line. These negative skewness patches are only weakly observed in the full and far angle stack lines.

In Zone 4, the skewness response is generally weakly negative, ranging between -0.3 and 0 in the full stack, with patches of positive skewness [generally > 1] throughout. The skewness response at the high amplitude BSR at the base of the GHSZ in Zone 4 is observed as stronger negative skewness [up to -0.5] in the near angle stack, slightly less negative in the full angle stack, and weakly negative [generally less than -0.1 to 0] skewness in the far angle stack. Along the low amplitude, discontinuous BSR at the northwest end of the seismic line, there is a weakly negative skewness [up to -0.5] response that is more apparent in the near angle stack, and approximately 0 to weakly negative [generally less than -0.1] skewness in the full and far angle stacks. Although the area below the GHSZ is outside the scope of this project, the skewness response is generally 0 to positive, with slightly more negative skewness observed in the near angle stack. Due to the contrast between the negative skewness response along the strong BSR in the full stack and FAS, and directly above the weak BSR in the NAS, in addition to the positive skewness directly above and below the BSR, the GHSZ is easily discernible from the interval underlying the BSR. Thus, using

To summarize the skewness response throughout the GHSZ, there are two zones of strong positive skewness [up to ~ 1.5 in the full stack] between roughly 3.4–3.59 (Zone 1 into Zone 2) seconds and from 3.8 to the base of the GHSZ (Zone 3). From 3.6 to 3.8 s (Zone 2), there is a 0 to negative skewness response [up to ~ -0.5 in the NAS] that is most evident in the near angle stack. Finally, at the base of the GHSZ/BSR (Zone 4), there is a weak to medium negative skewness response [up to ~ -0.5] that is strongest in the near angle stack.

Spectral kurtosis attribute

As mentioned in the previous skewness results, there is a similar kurtosis variation that is observed in the different angles. This kurtosis variation with angle is coined as “kurt-AVO” responses; however, it should be noted that this is not a typical AVO-type response, lined to amplitude changes with angle.

Within the one 1, kurtosis is generally negative, ranging between -1 at the ocean bottom to -1.5 throughout (Fig. 7). Immediate below the ocean bottom reflector is a thin interval of mixed strong positive to weak positive [up to 2.2 in the full stack and up to 1.3 in the NAS] from the full angle stack to the near angle stack, respectively. This thin, high kurtosis response appears in the southeastern half of the seismic line into the slope of the Hikurangi Channel and is strongest in the full angle stack, with values listed above. In Zone 2, the kurtosis is again generally negative, ranging from -1.5 to 0 , with stronger negatives observed in the NAS [up to -2] compared to the full stack and FAS [generally less than -0.1 up to $+3$ in some patches of positive kurtosis]. In the far angle stack, the kurtosis response follows a somewhat vertically stratified pattern which diminishes in the full and near angle stacks.

In Zone 3, below 3.8 s to the base of the GHSZ, the full and far angle stack show strong positive kurtosis [~ 2] kurtosis response directly above the high amplitude BSR. The far angle stack contains a broader and thicker extent of the positive kurtosis response compared to the full angle stack. The near angle stack only shows a very thin interval of strong positive kurtosis directly above the high amplitude BSR, with the majority of Zone 3 being negative to strong negative [around -2] kurtosis. Above the low amplitude, discontinuous BSR, there is an interval of negative kurtosis [approximately -1.5 in the full stack] that is more easily observed in the near and full stacks, and is weaker, discontinuous, and variable in the far angle stack. As previously mentioned for the skewness attribute, although the interval below the GHSZ is outside the scope of this project, the kurtosis response is predominately medium to strong negative, with patches of positive seen in all three angle stacks.

To summarize the kurtosis response, kurtosis proved to be quite variable throughout the GHSZ, especially with respect to variations observed across the angle stacks. In the full and far stacks, the kurtosis response showed negative kurtosis [-1.5 to 0] at the ocean bottom reflector and between 3.6 and 3.8 s (Zone 2), with a variable positive response [-1.5 to -1] above 3.6 s and directly below the ocean bottom (Zone 1). Between 3.8 and the base of the GHSZ/BSR (Zone 3), there was a zone of strong positive kurtosis [up to -2.0] in the full and far stacks, while the near stack showed mostly negative response. Kurtosis appears to be roughly vertically “stratified,” that is, it is closely laterally continuous (negative or positive) and these zones are separated by thin zero-value or weak positive/negative kurtosis.

Skewness and kurtosis crossplot

Crossplotting skewness versus kurtosis shows that there is a clear linear trend between the two attributes (Fig. 8). There is a strong positive correlation between the two attributes where skewness is low positive and kurtosis is low negative (in Zone 2 and in Zone 3 above the weak BSR) and where skewness is positive to strong positive and kurtosis is low positive (in Zone 1 toward the Hikurangi Channel and in Zone 3 above the strong BSR). Skewness and kurtosis were crossplotted using the same scales that defined the color bars for each respective attribute.

Supplemental attributes results

Only the results from the attributes calculated on the full stack seismic line are shown here, as it was outside the scope of the project to investigate the supplemental attributes’ variation across the different angle stacks. In the full stack line, RMS amplitude (Fig. 9b) response throughout the GHSZ is generally low [0 to 200], with the exception of the ocean bottom [375 to 550] and BSR [350 to 725], especially around the high-amplitude BSR, as would be expected for an amplitude-related attribute. There are slight variations throughout Zone 2 in the non-parallel, possible sediment wave reflectors, and slight enhancement of the weak BSR in Zone 4 where the BSR was discontinuous at the northwest end of the seismic line. Below the high-amplitude BSR seen in the seismic line, there is an interval of high [up to 480] RMS amplitude response, although the response is somewhat smeared.

The instantaneous frequency attribute ranges from 0 to 120 cycles/s with the highest frequency response at the ocean bottom, between 3.6 and 3.8 s (Zone 2), and along the high amplitude BSR (Zone 4). The instantaneous frequency was lowest [~ 10 to 25 Hz] in Zone 1 immediately below the ocean bottom reflector, and in Zone 3, with thin layers of medium to high frequency. The high frequency

response in Zone 2 roughly corresponds to the skewness and kurtosis attribute variations that were seen throughout that zone; there are higher frequencies observed in the interval corresponding to the negative skewness response throughout the sub-parallel reflectors. In both Zone 1, immediately below the ocean bottom, and in Zone 3, the low frequency variations correspond to positive skewness and kurtosis variations, with the exception of kurtosis in the near angle stack through Zone 3. Additionally, there are high frequency values [50 to 100 Hz] along the high amplitude BSR that correspond to negative skewness and kurtosis responses at the same interval. Frequency also has a medium-strength [30 to 35 Hz] attribute response along the weak/discontinuous and low amplitude BSR (as seen in Fig. 9c). Below the BSR, there are several higher frequency [~ 40 Hz] intervals, with the response falling in a more discrete expression than the RMS amplitude or envelope response.

The envelope attribute (Fig. 9d) response values ranged from 0 to 1800 . There were strong responses at the ocean bottom [700 to 1450] and along the high-amplitude BSR [700 to 1550], respectively, and throughout the GHSZ, envelope varied from around 0 to 200 . Envelope is generally vertically stratified throughout with no strong discernable patterns except for slightly higher envelope in Zone 2. Below the BSR (Zone 4), there were several increased-value [600 – 1200] envelope intervals. When analyzing the attribute response with angle, both envelope and RMS amplitude increased with angle from around 1000 to 1400 (unit of envelope) and 900 to 1100 (amplitude), respectively, although AVO-type responses were not comprehensively described for the supplemental attributes.

The sweetness attribute calculated on the full stack line shows weak variations throughout the GHSZ, with the ocean bottom and high amplitude BSR being the main strong positive [250 – 300] sweetness responses (Fig. 9e). Sweetness also generally follows the response pattern similar to the original seismic amplitude line. Below the BSR (Zone 4), there are several thin beds of high positive sweetness [200 – 300] following a similar expression as the amplitude and envelope attribute response sub-BSR.

Machine learning results

Based on the understanding of the geologic setting and seismic facies present in the Pegasus Basin, the SOM facies observed are correlated with the interpreted seismic facies, geologic features seen in the seismic data, or attribute observations. The four main seismic facies clusters recognized from the seismic attribute and SOM results are (1) high amplitude reflectors representing the ocean bottom facies (including a strong possible ocean bottom side lobe clustered in magenta) and BSR facies, (2) mixed siliciclastic facies representing the majority of the data as fairly continuous,

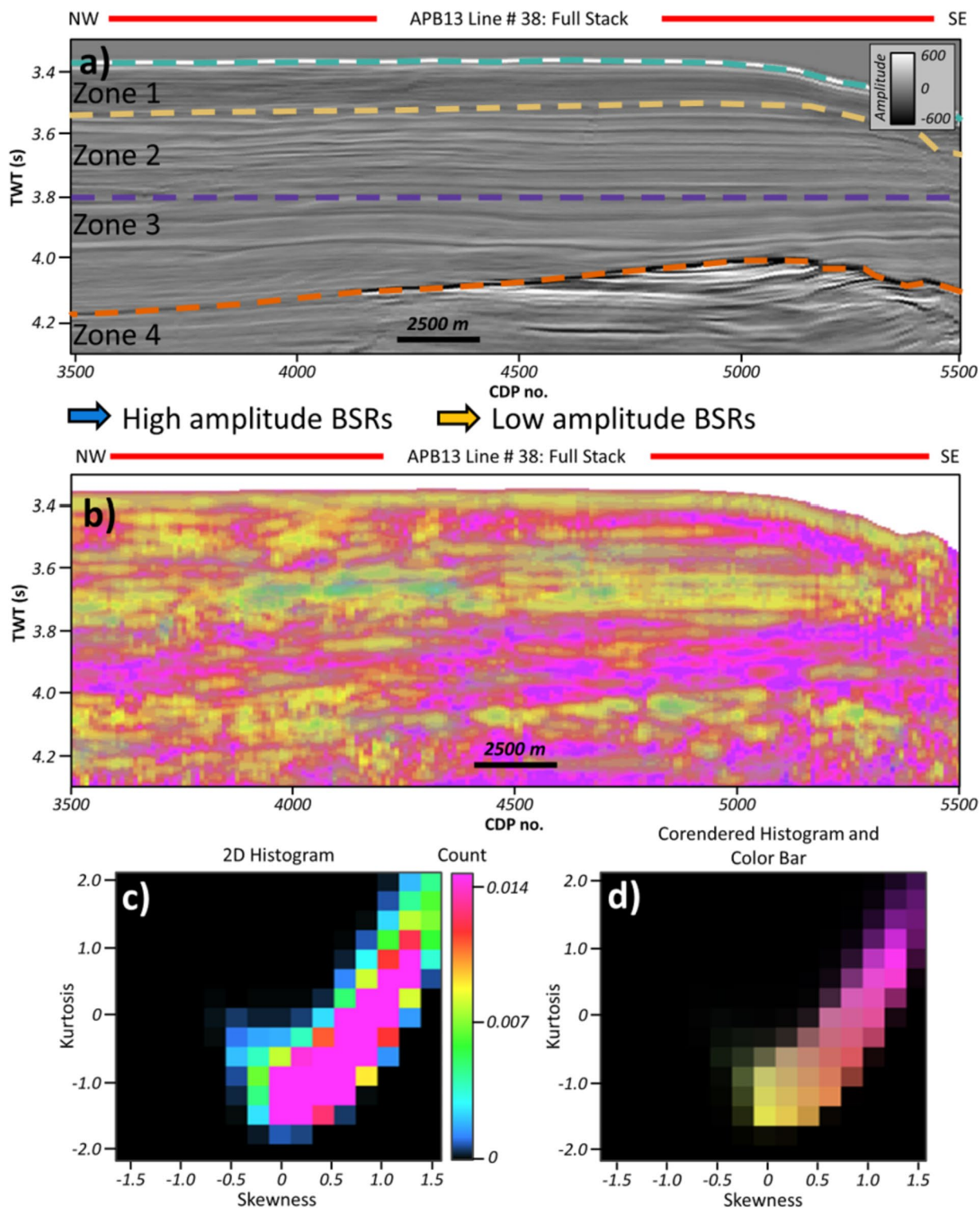
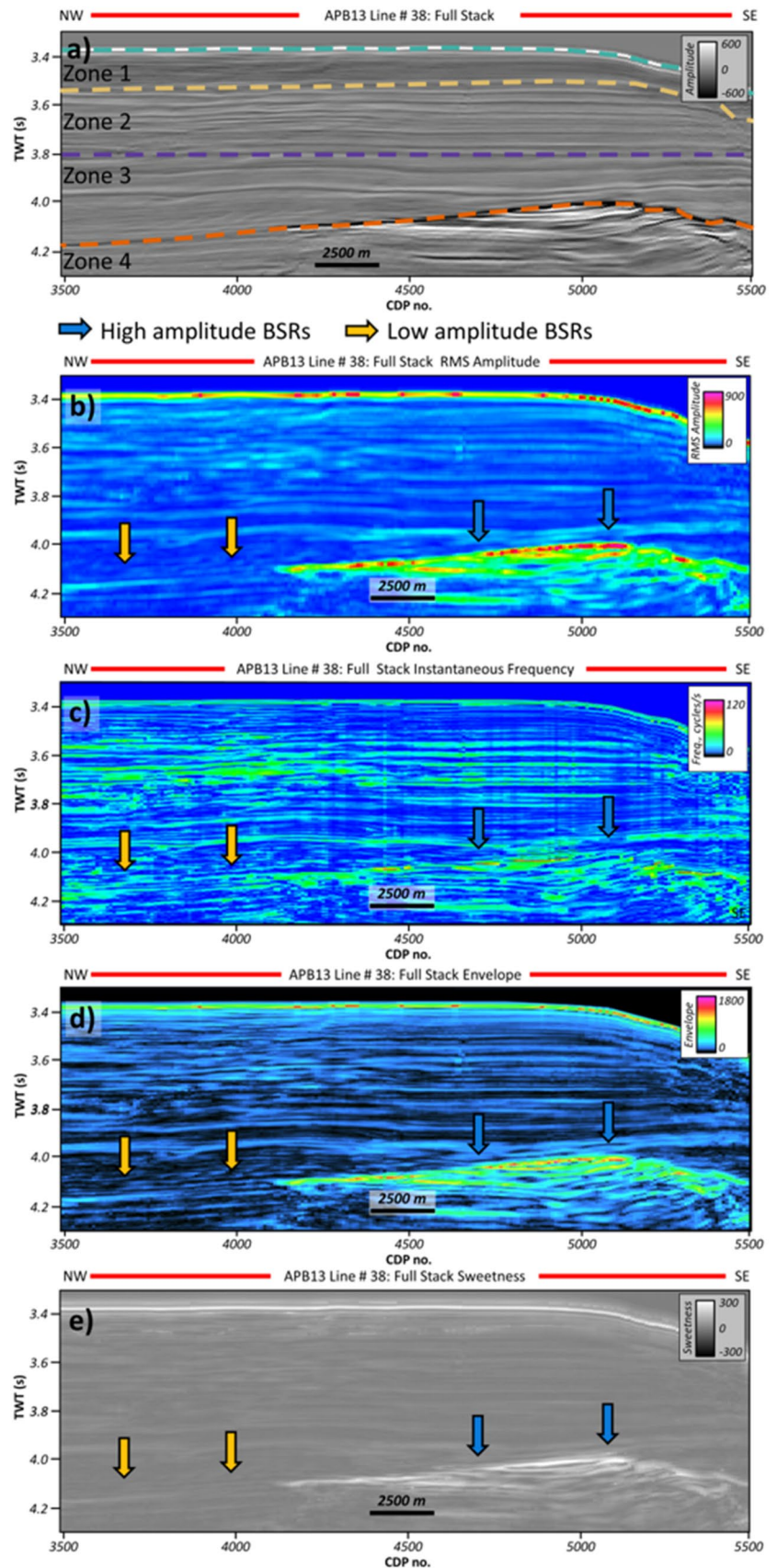


Fig. 8 **a** Full angle stack seismic line with high and low amplitude BSRs and Zones denoted by color, **b** Crossplot of kurtosis versus skewness calculated on the full stack seismic line, **c** 2D histogram showing count for kurtosis crossplotted against skewness, and **d**

Corendered histogram with 2D colorbar which corresponds to the colors shown in **b**. The histograms and 2D color map are used to determine the colors represented in Fig. 7b. See Fig. 4 for seismic line map locations

Fig. 9 **a** Full stack seismic line with high and low amplitude BSRs with Zones denoted by color, **b** RMS amplitude attribute, **c** Instantaneous frequency attribute, **d** Envelope attribute, and **e** Sweetness attribute. All attributes are calculated on the full stack seismic line with high and low amplitude BSRs shown by the arrows. See Fig. 4 for seismic line map locations



parallel reflectors, (3) the variable frequency facies that are most closely associated with spectral skewness and kurtosis and instantaneous frequency variations throughout Zones 1 and 3, and (4) the sediment wave facies.

Zone 1 for each of the angle stacks corresponds to a continuous ocean bottom reflector and then variable clustering for each of the three angle stacks (Fig. 9b – d). In the full stack, there are larger patches of the variable frequency facies toward the southeastern end of the seismic line, with few similar patches in the near, and almost none in the far angle stack. However, in the far angle stack (Fig. 10c), there are several beige clusters that follow the low-amplitude trough response in the 2D seismic line throughout Zone 1; these clusters are not observed in any other SOM angle stack. In Zone 2 the clustering is fairly continuous mixed siliciclastic facies with a few of the sediment wave facies clusters through the sub-parallel, possible sediment wave reflectors seen in the 2D seismic line; Zone 2 shows no significant variations among the angle stacks. Zone 3 contains both mixed siliciclastic facies and large patches of the variable frequency facies, which are more evident in the full stack than far and near, though the near stack patches appear more discrete than the other two angle stacks. Zone 4 contains the BSR shown by the magenta facies where the BSR was high amplitude in the 2D seismic, and is characterized by the mixed siliciclastic facies where the BSR was low amplitude in the 2D seismic. No data was classified below the BSR as the focus of this study was concentrated within the GHSZ.

Discussion

Attribute analysis

Spectral skewness attribute

Skewness is used to define the amount a dataset deviates from the normal distribution of a dataset (Fig. 3a). When comparing the spectral skewness results to the original seismic, it is observed that most of the spectral skewness variations are not closely related to observed seismic amplitude variations, with the exception of the sub-parallel sediment wave facies described in Zone 2. Zone 1 and Zone 3 contain the strongest positive skewness responses, which also correspond to lower frequencies described in the [instantaneous frequency attribute](#) section. The combination of positive skewness with low frequency values indicates that more attenuation is occurring across these intervals, especially compared to zones with high frequency and negative skewness. Positive skewness means the data is skewed toward the lower frequencies, which is confirmed by the low instantaneous frequency responses. The inverse of this is observed by comparing negative

skewness intervals with frequency, as well. Zone 2 and 4 both contain intervals of negative skewness in conjunction with higher instantaneous frequency, confirming that negatively skewed data do contain higher frequencies than positively skewed data. These effects demonstrate the frequency-dependent nature of attenuation. As discussed in a previous section, attenuation is expected to result in a loss of high frequencies over low frequencies (Raikes and White 1984), and additionally, higher attenuation rates with increasing hydrate saturation (Guerin and Goldberg, 2002; Chand and Minshull 2004; Dvorkin and Uden 2004, Riedel et al. 2010, etc.). The combination of a high amplitude BSR directly below strong positive skewness (representative of attenuation) is a strong case for gas hydrate accumulation at the base of the GHSZ causing noticeable attenuation of the seismic. Additionally, where increased positive skewness is observed in Zone 1 along the Hikurangi Channel, this may be an indication of shallow hydrate accumulation and localization throughout the Hikurangi Trough.

As described in the spectral skewness attribute [results](#) section, there is a stronger negative skewness response (that is, the amplitude of the skewness response is more negative) visible in the near angle stack compared to the full and far angle stacks. A negative skewness response (see Fig. 3) indicates that the seismic frequencies on the left end of the seismic spectrum are being attenuated more than those on the right, therefore skewing the spectrum to the right (which is negative skewness). With respect to the frequency content represented by the seismic amplitude spectrum over which skewness is calculated, this indicates that the *lower* frequencies are being attenuated more than the higher frequencies. When considering the expected attenuation within near angle stacks, there is a lower expected attenuation, and therefore, a higher frequency content, within the near angles (between 5–18°) since the seismic waves do not have to travel through the earth as much as to the far (between 32–45°) angles. This correlates with the skewness response that is visible across the different angle stacks. While the near angle stack shows a strong negative skewness response, the far angle stack shows a weak negative to 0 skewness response, which is likely due to attenuation by the earth causing an impact on the natural attenuation occurring within the hydrates themselves. This phenomenon is especially observed in Zone 2 which shows increasing negative skewness from the far to near angle stack while simultaneously reducing the positive skewness response from far to near angle stack (Fig. 6c and d).

In summary of the spectral skewness, although there exists some uncertainty due to lack of well data and depths of hydrate accumulation, skewness proves to be useful for distinguishing zones in the seismic which are experiencing reduction in frequency and amplitude, and based on evidence of gas hydrates occurring throughout the Pegasus

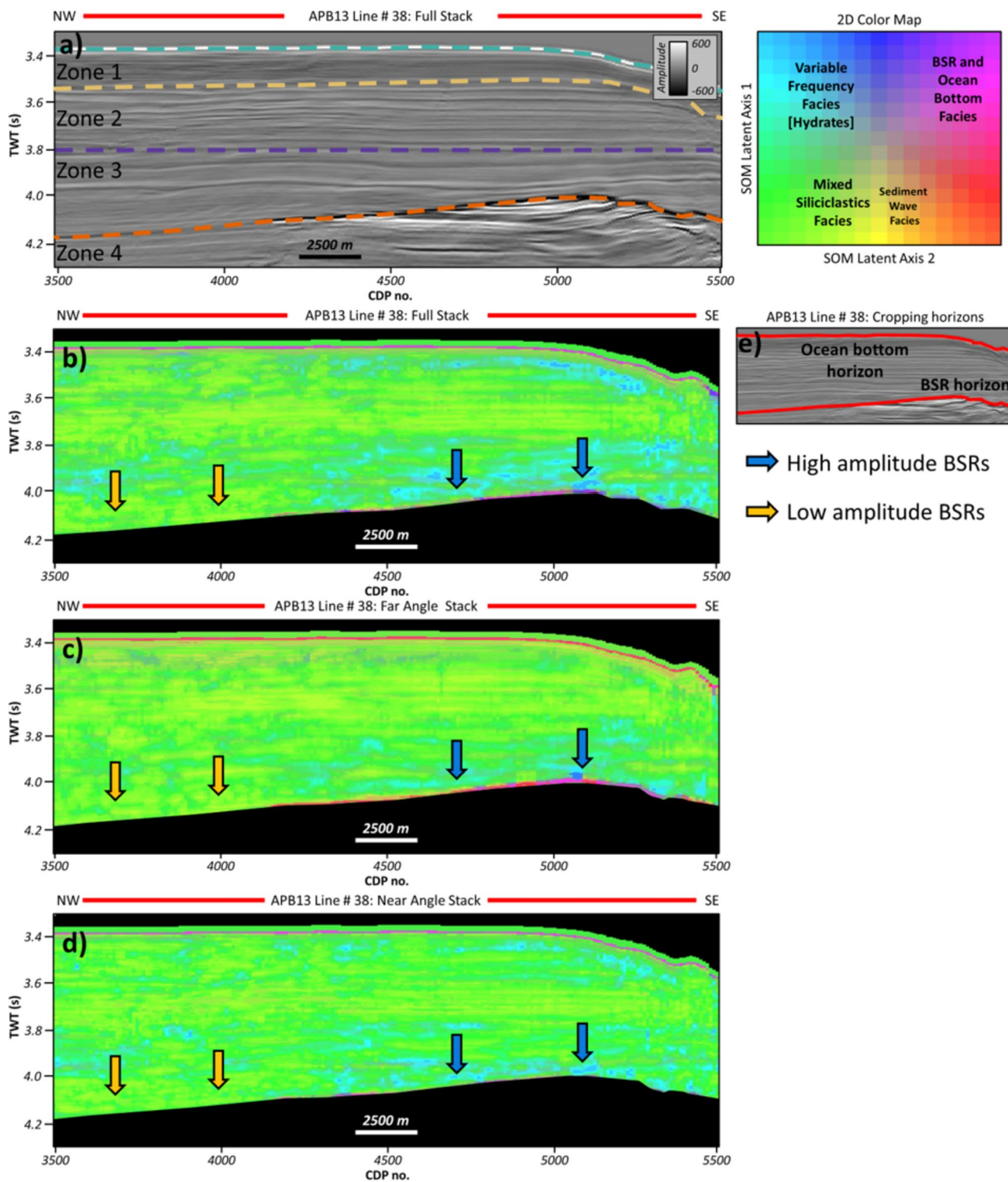


Fig. 10 **a** Full stack seismic line showing high and low amplitude BSRs with the Zones denoted by color, **b** SOM results calculated from the full stack seismic line between the ocean bottom and BSR horizons, **c** SOM results calculated from the far angle stack seismic line between the ocean bottom and BSR horizons, **d** SOM results calculated from the near angle stack seismic line between the ocean bot-

tom and BSR horizons, **e** Ocean bottom horizon and BSR horizon for vertical window cutoff. 2D colorbar showing the interpreted facies represented in b, c, and d. The facies interpreted to be hydrates are highlighted in the teal-blue colors. See Fig. 4 for seismic line map locations

Basin as discussed in Sect. 2.3, this attenuation is tied to gas hydrates in the GHSZ.

Spectral kurtosis attribute

Kurtosis is a statistical measure that defines the “tailedness” of dataset from the mean in a normal distribution (Fig. 3b) of a dataset. With kurtosis, there is a kurt-AVO response occurring similar to the skew-AVO response described previously. The kurtosis response in Zone 3 is strong positive in the far angle stack, whereas in the near angle stack throughout the same zone, the kurtosis response is strong negative; indeed, the values are curiously nearly opposite in the two different angle stacks. In relationship to the theory of kurtosis, positive kurtosis indicates that there are few outliers and a higher peaked-ness to the data as measured from the spectrum at that sample location, while negative kurtosis indicates more outliers and a lower peaked-ness in the data as measured from the spectrum at that sample location. So, comparing that to the frequency content of the data, that could mean that, where there is a higher kurtosis response in the far angles, the frequency content contains a narrower spectrum or bandwidth of frequencies compared to the normal distribution. On the other hand, the negative kurtosis implies that there is a broader distribution or bandwidth of frequencies, both high *and* low, when compared to the normal distribution of the data.

In the full and far angle stacks, the strong positive kurtosis response above the high amplitude BSR indicates a narrower bandwidth of data compared to the overlying negative kurtosis in Zone 2. Zone 3 also contains lower frequency, which may indirectly be driving the bandwidth and subsequently, kurtosis response. In the near angle stack, Zone 3, and indeed, nearly the entire GHSZ, contains negative kurtosis. The positive kurtosis in Zone 3 in both the full and far angle stacks is likely due to gas hydrates attenuating the seismic spectrum and reducing the bandwidth of the data. As discussed in Sect. 1.1 and 1.2, hydrates are shown to increase the rigidity of the rock frame while simultaneously increasing attenuation, which is somewhat unexpected. While the aim of this paper is not to address the exact mechanism of attenuation in the Pegasus Basin, it is clear that attenuation is occurring, and can be linked to other phenomenon that support gas hydrate accumulation in the GHSZ, such as the BSR. The mechanism of negative kurtosis in Zone 3 in the near angle stack is more difficult to understand, but likely is due to some interaction between attenuation from hydrates and attenuation due to angle; however, this exact response is not well understood.

In summary, kurtosis delineated two primary zones of kurtosis variation, with a third zone with slight variation that may be correlated with gas hydrates. Since hydrates have been recovered within the shallow sediments of the

Pegasus Basin (see Fig. 4), there is likelihood the strong attenuation in Zone 1 may correspond to gas hydrate accumulation, as well as the strong kurt-AVO responses observed in Zone 3 above the strong BSR. Although there is some uncertainty due to lack of well data to confirm intervals with hydrate accumulation, based on the understanding of the GHSZ in the Pegasus Basin, the kurtosis response and variation is likely due to discontinuous zones of gas hydrate accumulation.

Spectral attribute considerations and summary

The strong positive spectral variations observed in Zone 1 may also be due to hydrate accumulation, which is known to occur in the shallow subsurface and has been recovered by crop cores in the Pegasus Basin (see Fig. 4 and Bialas 2011). Although there are indications that hydrates may exist in the shallow subsurface of the GHSZ, the skewness and kurtosis attributes show the strongest response toward the base of the GHSZ, which is most indicative of hydrates, while there is a zone of lower skewness seen in the western extents in the full and angle stacks, which does not correspond to any particular amplitude feature or anomaly. It seems more plausible that there are discontinuous zones or patches of hydrates throughout the GHSZ rather than one solid hydrate-filled sediment package; indeed, studies have shown that hydrates can occur in discontinuous intervals of the subsurface of the GHSZ (Cordon et al. 2006; Guerin and Goldberg, 2002).

Based on the results of the skewness and kurtosis cross-plot (Fig. 8), there is a clear positive correlation between skewness and kurtosis. The strongest positive correlation between skewness and kurtosis demonstrates high attenuation, and these areas, particularly Zone 1 (along the Hikurangi Trough) and Zone 3, are interpreted to represent gas hydrate accumulations. Additionally, these areas generally correspond to where the “attenuation” facies were classified in the SOM, making another case for hydrate accumulation represented by high attenuation and frequency reduction. The simple cross-correlation is useful as an additional visual representation of how these attributes are related to each other and potential zones of hydrate accumulation, as well as being a simple method to quality control check the results and interpretation from the machine learning.

Lastly, based on the observations from the spectral attributes in the Pegasus Basin, these attributes have the potential to be considered a type of direct hydrate indicator, similar to common DHIs. Although there are some uncertainties in the exact locations of gas hydrates due to lack of well data in the Pegasus Basin, even well-accepted DHIs do not explicitly confirm the existence of hydrocarbons, but rather indicate hydrocarbon existence based on the attribute theory, concepts, and thorough, scientific interpretation of the attribute

response. In the same way, spectral attributes give a response based on the statistical shape of the seismic spectrum and, when interpreting that in terms of attenuation specifically in a gas hydrate setting, can indicate zones with gas hydrates.

Supplemental attributes

The results from the instantaneous frequency attribute show high frequency variations at the same locations where there is a negative spectral skewness response, indicating that these variations are related to frequency responses, rather than changes in the amplitude volume of the seismic or lithology. This is consistent with expectations that high frequencies are being attenuated throughout the GHSZ, and the corresponding skewness and kurtosis attributes show (positive) responses that indicate lower peak frequencies compared to a non-hydrate filled zone. The results from the envelope and RMS amplitude generally correspond to the high amplitude seen in the seismic amplitude volume. Below the BSR, the RMS amplitude, envelope, and sweetness responses all point toward hydrocarbon accumulation. The sweetness attribute, for example, which is calculated from the frequency and envelope attribute and often used to delineate hydrocarbon-filled sands (or “sweet” spots), shows a strong positive response below the high amplitude BSR; this response is likely due to trapped free gas below the GHSZ. The trapped free gas creates the strong impedance contrast between the hydrate-filled sediments in the GHSZ and the free gas in the zone below, therefore creating a strong BSR. RMS amplitude and envelope are also commonly used to indicate hydrocarbon accumulation, creating a strong case for free gas below the GHSZ.

While the supplemental attributes proved useful for highlighting the BSR at the base of the GHSZ, these attributes proved to be less indicative of attenuation itself, and show fewer correlations between their attribute response and the interesting spectral attribute responses and variations observed between the angle stacks. Nevertheless, they do show a clear delineation between amplitude- and frequency-related responses and what attributes are most appropriate for quantifying attenuation, in addition to providing the necessary supplemental attributes for machine learning.

Self-organizing maps

At its core, self-organizing maps is a dimensionality-reduction technique that allows a researcher to input multiple attributes into a machine learning algorithm and analyze the output feature maps or clusters of the data. The implications of using SOM to analyze attenuation throughout the GHSZ is that there will be influence from not only the spectral shape attributes and their variations throughout the GHSZ, but also from the supplemental attributes, which proved less

useful for highlighting attenuation effects. Therefore, it is expected that while the combination of input attributes will give clues to the attenuation response through the GHSZ, attributes that use strictly frequency or attenuation attributes may prove more robust in delineating the subtle changes observed by the spectral shape attributes.

The primary clusters in the SOM are the ocean bottom facies and BSR facies cluster, the mixed siliciclastic facies clusters, the variable frequency facies clusters, and where present, the sediment wave facies clusters. Although each attribute is weighted equally when computing the SOM throughout the GHSZ, certain SOM clusters are created because individual attributes have stronger or weaker responses in particular areas. For example, the RMS amplitude, envelope, sweetness, and instantaneous frequency each have a strong and relatively distinct ocean bottom and BSR response, whereas the spectral skewness and kurtosis have less distinct responses along the BSR, although fairly consistent along the ocean bottom. Therefore, the strong ocean bottom and BSR facies cluster is due largely to the supplemental attribute’s input rather than strong responses from the spectral attributes. Likewise, the variable frequency facies is closer related to variations in the spectral attributes and instantaneous frequency attribute than the RMS, envelope, or sweetness attributes. In general, the results from the SOM are useful for delineating amplitude-related features from frequency-related features, and as was previously discussed, indicating attenuation where frequency and spectral attributes showed strong responses.

Although more work could be done to enhance the SOM classification of hydrates through the GHSZ, especially through implementation of other frequency- or attenuation-related attributes, the SOM models presented here are shown to distinguish two primary zones (Zone 1 and 3) of high attenuation or frequency variations, and one zone (Zone 2) related more closely to underlying geologic features (sediment waves).

Conclusions

Gas hydrates are a complex and, in many areas, poorly imaged geologic phenomenon that exist in marine and permafrost settings. In the APB13 dataset from the Pegasus Basin offshore the east coast of the North Island of New Zealand, gas hydrates are indirectly indicated from both clear and discontinuous BSRs, in addition to methane hydrate-bearing drop cores recovered throughout the western Pegasus Basin. However, due to the inconsistent nature of BSRs, other methods are needed to identify gas hydrates within the gas hydrate stability zone. Attenuation, closely associated with hydrate filling the pore-space within the GHSZ, measured by statistical attributes - skewness and

kurtosis is proposed as a method to identify hydrates in the absence of BSRs. These statistical attributes, in combination with instantaneous and RMS amplitude attributes, are used to determine the attenuation response and variation within the GHSZ of the APB-13 2D seismic dataset, and used as input into a SOMs machine learning algorithm. The results from the attribute analysis show that the frequency-related attributes - instantaneous frequency and the spectral/statistical attributes skewness and kurtosis - are able to highlight attenuation throughout the hydrate-saturated zone within the GHSZ. Additionally, based on these attribute responses, it appears that the hydrates in the Pegasus Basin are discontinuous throughout the GHSZ, as evidence by a high skewness and kurtosis response directly above the high amplitude BSRs overlain by a zone of negative skewness and kurtosis, which may be indicative of a hydrate-free interval. As the frequency/spectral-related attribute response/variation in Zone 3 does not correspond to any noticeable amplitude attribute variation or appear within the original seismic amplitude volume, we conclude that it is related to attenuation of frequencies due to the gas hydrates.

Based on the SOM results, there was a corresponding response at the areas where the frequency attributes showed peak responses/variability. As expected from the skew-AVO and kurt-AVO analysis of the spectral attributes, the variations often reach their peak with angle in the SOM results. Comparing the two SOM cases, it is observed that running machine learning between a smaller interval allows for more discrete classification of data, and it is therefore recommended to calculate attributes and machine learning implementation across a narrower user-defined window or cropping horizons.

From this study, it is shown that statistical/spectral attributes - skewness and kurtosis - are able to measure the attenuation variations within the GHSZ zone of the Pegasus Basin APB13 2D seismic dataset. Based on these results and interpretations, it is recommended that spectral attributes be applied to other areas that have suspected gas hydrates but perhaps sparse BSRs or well data, in addition to settings with confirmed gas hydrates and well or core data. Future work, including synthetic modeling of hydrates and attributes, will be useful for determining how saturation of hydrates and varying lithologies impacts attenuation response, and provide more quantitative means to measure attenuation in seismic data.

Acknowledgements The AASPI (Attribute Assisted Seismic Processing and Interpretation) software used to compute many of the seismic attributes and all the machine learning models for this research was provided by the AASPI consortium at the University of Oklahoma. The Petrel license and software packages used for visualization and computing the sweetness attribute were provided by Schlumberger. The authors thank the AASPI research group at the University of Oklahoma, and Dr. Kurt Marfurt for his technical feedback.

Author contributions EJ: Wrote the main manuscript text and prepared each of the figures within the text. HB: Provided technical feedback on figures, seismic attributes, geophysical setting and methodology. TH: Provided technical feedback on the software used to compute the seismic attributes and machine learning. All authors reviewed the manuscript.

Funding This research was funded by an American Chemical Society (ACS) Petroleum Research Fund (PRF) grant to Dr. Heather Bedle at the University of Oklahoma School of Geosciences.

Data availability The Pegasus Basin APB13 Seismic Survey was provided by the New Zealand Government's Department of Petroleum & Minerals.

Declarations

Competing interests The authors declare no competing interests.

Ethical approval and consent to participate Not applicable.

Consent for publication Not applicable.

7. References

- AASPI Researchers (2020) Volumetric Self-organizing maps for 3D seismic facies analysis - Program som3d, University of Oklahoma Mewbourne College of Earth and Energy, <https://mcee.ou.edu/aaspi/documentation.html>. Accessed 02/10/2022
- Bedle H (2019) Seismic attribute enhancement of weak and discontinuous gas hydrate bottom-simulating reflectors in the Pegasus Basin, New Zealand. Interpretation 7:SG11–SG22. <https://doi.org/10.1190/INT-2018-0222.1>
- Berndt C, Büinz S, Clayton T et al (2004) Seismic character of bottom simulating reflectors: examples from the mid-norwegian margin. Mar Pet Geol 21:723–733. <https://doi.org/10.1016/j.marpetgeo.2004.02.003>
- Best AI, Priest JA, Clayton CRI (2010) A resonant column study of the seismic properties of methane-hydrate-bearing sand. In: Riedel M et al (ed) Geophysical Characteristics of Gas Hydrates. Society of Exploration Geophysicists Geophysical Developments Series No. 14. pp 337–347 <https://doi.org/10.1190/1.9781560802197>
- Bialas J (2011) FS SONNE Cruise Report SO-214 NEMESYS. IMF-GEOMAR Rep 47. https://doi.org/10.3289/ifm-geomar_rep_47_2011
- Biot MA (1956a) Theory of propagation of elastic waves in a fluid saturated, porous solid. I. low-frequency range. J Acoust Soc Am 28:168–178
- Biot MA (1956b) Theory of propagation of elastic waves in a fluid saturated porous solid. II. High frequency range. J Acoust Soc Am 28:179–191
- Bland KJ, Uruski CI, Isaac MJ (2015) Pegasus Basin, eastern New Zealand: a stratigraphic record of subsidence and subduction, ancient and modern. NZ J Geol Geophys 58:319–343. <https://doi.org/10.1080/00288306.2015.1076862>
- Boswell R, Hutchinson D (2005) Changing perspectives on the resource potential of methane hydrates. NETL Methane Hydrate Newsletter
- Castagna JP, Sun S, Siegfried RW (2003) Instantaneous spectral analysis: detection of low-frequency shadows associated with hydrocarbons. Lead Edge 22:120–127. <https://doi.org/10.1190/1.1559038>
- CGG Services (Singapore) Pte. Ltd, Anadarko New Zealand Ltd (2014) Seismic Data Processing Report – APB-13-2D Pegasus

- Basin 2D PEP54861; NZP&M, Ministry of Business, Innovation & Employment (MBIE), New Zealand. Unpublished Petroleum Report PR5170
- Chand S, Minshull T (2004) The effect of hydrate content on seismic attenuation: a case study for Mallik 2L-38 well data, Mackenzie delta, Canada. *Geophys Res Lett* 31:L14609. <https://doi.org/10.1029/2004GL020292>
- Chenin J, Bedle H (2020) Multi-attribute machine learning analysis for weak BSR detection in the Pegasus Basin, Offshore New Zealand. *Mar Geophys Res* 41:21. <https://doi.org/10.1007/s11001-020-09421-x>
- Chopra S, Marfurt KJ (2007) Seismic attributes for Prospect Identification and Reservoir characterization. Society of Exploration Geophysicists
- Clairmont R, Bedle H, Marfurt K, Wang Y (2021) Seismic attribute analyses and attenuation applications for Detecting Gas Hydrate Presence. *Geosciences* 11:450. <https://doi.org/10.3390/geosciences111110450>
- Collier T (2015) The Geology of Pegasus Basin Based on Outcrop Correlatives in Southern Wairarapa and Northeastern Marl-Borough, New Zealand. Master's Thesis, Victoria University of Wellington, Auckland, New Zealand, 2015. Available online: <http://hdl.handle.net/10063/4831> (accessed on 10 October 2022)
- Cordon I, Dvorkin J, Mavko G (2006) Seismic reflections of gas hydrate from perturbational forward modeling. *Geophysics* 71:F165–F171. <https://doi.org/10.1190/1.2356909>
- Davies RJ, Maqueda MAM, Li A, Ireland M (2021) Climatically driven instability of marine methane hydrate along a canyon-incised continental margin. *Geology* 49:973–977. <https://doi.org/10.1130/G48638.1>
- Davogustto O, de Matos MC, Cabarcas C et al (2013) Resolving subtle stratigraphic features using spectral ridges and phase residues. *Interpretation* 1:SA93–SA108. <https://doi.org/10.1190/INT-2013-0015.1>
- de Matos MC, Davogustto O, Cabarcas C, Marfurt K (2012) Improving reservoir geometry by integrating continuous wavelet transform seismic attributes. SEG Technical Program expanded abstracts 2012. Society of Exploration Geophysicists, pp 1–5
- DeMets C, Gordon RG, Argus DF (2010) Geologically current plate motions. *Geophys J Int* 181:1–80. <https://doi.org/10.1111/j.1365-246X.2009.04491.x>
- Dev A, McMechan GA (2010) Interpreting structural controls on hydrate and free-gas accumulation using well and seismic information from the Gulf of Mexico. *Geophysics* 75:B35–B46. <https://doi.org/10.1190/1.3282680>
- Dvorkin JP, Mavko G (2006) Modeling attenuation in reservoir and nonreservoir rock. *Lead Edge* 25:194–197. <https://doi.org/10.1190/1.2172312>
- Dvorkin J, Uden R (2004) Seismic wave attenuation in a methane hydrate reservoir. *Lead Edge* 23:730–732. <https://doi.org/10.1190/1.1786892>
- Dvorkin J, Gutierrez MA, Grana D (2014) *Seismic Reflections of Rock Properties*. Cambridge University Press, England. <https://doi.org/10.1017/CBO9780511843655>
- Englezos P (1993) Clathrate hydrates. *Ind Eng Chem Res* 32:1251–1274
- Fraser DRA, Gorman AR, Pecher IA et al (2016) Gas hydrate accumulations related to focused fluid flow in the Pegasus Basin, southern Hikurangi Margin, New Zealand. *Mar Pet Geol* 77:399–408. <https://doi.org/10.1016/j.marpetgeo.2016.06.025>
- Gas Hydrates R&D Program US Department of Energy, Factsheet (2020) <https://www.energy.gov/fecm/gas-hydrates>. Accessed 2 September 2023
- Grossmann A, Morlet J (1984) Decomposition of hardy functions into square integrable wavelets of constant shape. *SIAM J Math Anal* 15:726–736
- Guerin G, DS Goldberg (2002) Sonic waveform attenuation in gas hydrate-bearing sediments from the Mallik 2L-38 research well, Mackenzie Delta, Canada. *J Geophys Res* 107:2088. <https://doi.org/10.1029/2001JB000556>
- Hammerschmidt EG (1934) Formation of gas hydrates in natural gas transmission lines. *Ind Eng Chem* 26:851–855
- Hart BS (2008) Channel detection in 3-D seismic data using sweetness. *Bulletin* 92:733–742. <https://doi.org/10.1306/02050807127>
- Hilterman F, Van Schuyver C (2003) Seismic wide-angle processing to avoid NMO stretch. SEG Technical Program Expanded Abstracts 2003. Society of Exploration Geophysicists, Oklahoma, pp 215–218
- Holbrook WS, Hoskins H, Wood WT et al (1996) Methane hydrate and Free Gas on the Blake Ridge from Vertical Seismic Profiling. *Science* 273:1840–1843. <https://doi.org/10.1126/science.273.5283.1840>
- Hornbach MJ, Holbrook WS, Gorman AR et al (2003) Direct seismic detection of methane hydrate on the Blake Ridge. *Geophysics* 68:92–100. <https://doi.org/10.1190/1.1543196>
- Hussein M, Stewart RR, Sacrey D et al (2021) Unsupervised machine learning using 3D seismic data applied to reservoir evaluation and rock type identification. *Interpretation* 9:T549–T568. <https://doi.org/10.1190/INT-2020-0108.1>
- King SE (2017) The Tectonic Evolution of Pegasus Basin and the Hikurangi Trench, offshore New Zealand. Master's Thesis, Colorado School of Mines, Golden, Colorado, 2017
- Klimentos T, McCann C (1990) Relationships among compressional wave attenuation, porosity, clay content, and permeability in sandstones. *Geophysics* 55:998–1014. <https://doi.org/10.1190/1.1442928>
- Kohonen T (1982) Self-organizing formation of topologically correct feature maps. *Biol Cybern* 43:59–69. <https://doi.org/10.1007/BF00337288>
- Kohonen T (1990) The self-organizing map. *Proc IEEE* 78(9):1464–1480
- Kroeger KF, Plaza-Faverola A, Barnes PM, Pecher IA (2015) Thermal evolution of the New Zealand Hikurangi subduction margin: impact on natural gas generation and methane hydrate formation – A model study. *Mar Pet Geol* 63:97–114. <https://doi.org/10.1016/j.marpetgeo.2015.01.020>
- La Marca K, Bedle H (2021) Deepwater seismic facies and architectural element interpretation aided with unsupervised machine learning techniques: Taranaki basin, New Zealand. *Mar Pet Geol* 136:105427. <https://doi.org/10.1016/j.marpetgeo.2021.105427>
- La Marca K, Silver C, Bedle H, Slatt R (2019) Seismic facies identification in a deepwater channel complex applying seismic attributes and unsupervised machine learning techniques. A case study in the Tarinaki Basin, New Zealand. 89th Annual International Meeting SEG Expanded abstracts:2059–2063. <https://doi.org/10.1190/segam2019-3216705.1>
- Lewis KB, Pantin HM (2002) Channel-axis, overbank and drift sediment waves in the southern Hikurangi Trough, New Zealand. *Mar Geol* 192:123–151. [https://doi.org/10.1016/S0025-3227\(02\)00552-2](https://doi.org/10.1016/S0025-3227(02)00552-2)
- Lewis KB, Collot J, Lallemand SE (1998) The dammed Hikurangi Trough: a channel-fed trench blocked by subducting seamounts and their wake avalanches (New Zealand–France GeodyNZ Project). *Basin Res* 10:441–468. <https://doi.org/10.1046/j.1365-2117.1998.00080.x>
- Li F, Zhou H, Li L, Marfurt KJ (2015) Seismic spectral attributes of apparent attenuation: part 1 - methodology. SEG Technical Program expanded abstracts 2015. Society of Exploration Geophysicists, New Orleans, Louisiana, pp 1966–1970
- Li F, Verma S, Zhou H et al (2016) Seismic attenuation attributes with applications on conventional and unconventional reservoirs. *Interpretation* 4:SB63–SB77. <https://doi.org/10.1190/INT-2015-0105.1>

- Liu P, Huang H, Hu L et al (2022) Hydrate attenuation characteristics based on the patchy-saturation model. *Front Earth Sci* 10:831405. <https://doi.org/10.3389/feart.2022.831405>
- Lubo-Robles D, Bedle H, Marfurt KJ, Pranter MJ (2023) Evaluation of principal component analysis for seismic attribute selection and self-organizing maps for seismic facies discrimination in the presence of gas hydrates. *Mar Pet Geol* 150:106097. <https://doi.org/10.1016/j.marpetgeo.2023.106097>
- Majumdar U, Cook AE, Shedd W, Frye M (2016) The connection between natural gas hydrate and bottom-simulating reflectors. *Geophys Res Lett* 43:7044–7051. <https://doi.org/10.1002/2016GL069443>
- Maslin M, Owen M, Betts R et al (2010) Gas hydrates: past and future geohazard? *Phil Trans R Soc A* 368:2369–2393. <https://doi.org/10.1098/rsta.2010.0065>
- Peyton L, Bottjer R, Partyka G (1998) Interpretation of incised valleys using new 3-D seismic techniques: a case history using spectral decomposition and coherency. *Lead Edge* 17:1294–1298. <https://doi.org/10.1190/1.1438127>
- Plaza-Faverola A, Klaeschen D, Barnes P, Pecher I, Henrys S, Mountjoy J (2012) Evolution of fluid expulsion and concentrated hydrates zones across the southern Hikurangi subduction margin, New Zealand: an analysis for depth migrated seismic data. *AGU* 13:8. <https://doi.org/10.1029/2012GC004228>
- Raikes SA, White RE (1984) Measurements of Earth Attenuation from Downhole and Surface Seismic Recordings*. *Geophys Prospect* 32:892–919. <https://doi.org/10.1111/j.1365-2478.1984.tb00745.x>
- Riedel M, Willoughby EC, Chopra S (2010) Geophysical characteristics of gas hydrates. 14. Society of Exploration Geophysicists Geophysical Developments Series No. <https://doi.org/10.1190/1.9781560802197>
- Sahoo SK, North LJ, Marín-Moreno H et al (2019) Laboratory observations of frequency-dependent ultrasonic P-wave velocity and attenuation during methane hydrate formation in Berea sandstone. *Geophys J Int* 219:713–723. <https://doi.org/10.1093/gji/ggz311>
- Satyavani N, Sain K, Lall M, Kumar BJP (2008) Seismic attribute study for gas hydrates in the Andaman Offshore India. *Mar Geophys Res* 29:167–175. <https://doi.org/10.1007/s11001-008-9053-x>
- Sharma A (2020) Skewness & Kurtosis Simplified. Medium, Towards Data Science website, <https://towardsdatascience.com/skewness-kurtosis-simplified-1338e094fc85>. Accessed 16 February 2023
- Singh SC, Minshull TA, Spence GD (1993) Velocity structure of a gas hydrate reflector. *Science* 260:204–207. <https://doi.org/10.1126/science.260.5105.204>
- Sloan ED (2003) Fundamental principles and applications of natural gas hydrates. *Nature* 426:353–359. <https://doi.org/10.1038/nature02135>
- Taner MT, Koehler F, Sheriff RE (1979) Complex seismic trace analysis. *Geophysics* 44:1041–1063. <https://doi.org/10.1190/1.1440994>
- Taylor MH, Dillon WP, Pecher IA (2000) Trapping and migration of methane associated with the gas hydrate stability zone at the Blake Ridge Diapir: new insights from seismic data. *Mar Geol* 164:79–89. [https://doi.org/10.1016/S0025-3227\(99\)00128-0](https://doi.org/10.1016/S0025-3227(99)00128-0)
- Shibley TH, Houston MH (1979) Seismic evidence for widespread possible gas hydrate horizons on continental slopes and rises. *Bulletin*. 63: <https://doi.org/10.1306/2F91890A-16CE-11D7-8645000102C1865D>
- US Energy Information Administration (2020) Annual Energy Outlook. <https://www.eia.gov/aeo>. Accessed 2 September 2023
- Wang Y, Bedle H, Marfurt K (2023) Seismic stratigraphy and attenuation of gas-hydrate zones within the Hikurangi and Gondwana Margins, eastern New Zealand. *Geophys J Int*. <https://doi.org/10.1093/gji/ggad148>
- White JE (1975) Computed seismic speeds and attenuation in rocks with partial gas saturation. *Geophysics* 40:224–232. <https://doi.org/10.1190/1.1440520>
- Zhan L, Matsushima J (2018) Frequency-dependent P-wave attenuation in hydrate-bearing sediments: a rock physics study at Nankai Trough, Japan. *Geophys J Int* 214:1961–1985. <https://doi.org/10.1093/gji/ggy229>
- Zhao T, Jayaram V, Roy A, Marfurt KJ (2015) A comparison of classification techniques for seismic facies recognition. *Interpretation* 3:SAE29–SAE58. <https://doi.org/10.1190/INT-2015-0044.1>
- Zhao T, Zhang J, Li F, Marfurt KJ (2016) Characterizing a turbidite system in Canterbury Basin, New Zealand, using seismic attributes and distance-preserving self-organizing maps. *Interpretation* 4:SB79–SB89. <https://doi.org/10.1190/INT-2015-0094.1>
- Zhao T, Li F, Marfurt KJ (2018) Seismic attribute selection for unsupervised seismic facies analysis using user-guided data-adaptive weights. *Geophysics* 83:O31–O44. <https://doi.org/10.1190/geo2017-0192.1>

Publisher's note Springer Nature remains neutral with regard to jurisdictional claims in published maps and institutional affiliations.

Springer Nature or its licensor (e.g. a society or other partner) holds exclusive rights to this article under a publishing agreement with the author(s) or other rightsholder(s); author self-archiving of the accepted manuscript version of this article is solely governed by the terms of such publishing agreement and applicable law.